Translational contributions to tissue-specificity in rhythmic and constitutive gene expression

Violeta Castelo-Szekely[1], Alaaddin Bulak Arpat[1,2], Peggy Janich[1], David Gatfield[1,*]

[1] Center for Integrative Genomics, University of Lausanne, Génopode, 1015 Lausanne, Switzerland and [2] Vital-IT, Swiss Institute of Bioinformatics, Génopode, 1015 Lausanne, Switzerland

[*] corresponding author

authors' email addresses:
Violeta.CasteloSzekely@unil.ch, bulak.arpat@unil.ch, peggy.janich@krebsliga.ch, david.gatfield@unil.ch

Abstract

BACKGROUND: The daily gene expression oscillations that underlie mammalian circadian rhythms show striking tissue differences and involve post-transcriptional regulation. Both aspects remain poorly understood. We have used ribosome profiling to explore the contribution of translation efficiency to temporal gene expression in kidney, and contrasted our findings with liver data available from the same mice.

RESULTS: Rhythmic translation of constantly abundant mRNAs affected largely non-overlapping transcript sets with distinct phase clustering in the two organs. Moreover, tissue differences in translation efficiency modulated the timing and amount of protein biosynthesis from rhythmic mRNAs, consistent with organ-specificity in clock output gene repertoires and rhythmicity parameters. Our comprehensive datasets provided insights into translational control beyond temporal regulation. Between tissues, many transcripts showed differences in translation efficiency, which were, however, of markedly smaller scale than mRNA abundance differences. Tissue-specific changes in translation efficiency were associated with specific transcript features and, intriguingly, globally counteracted and compensated transcript abundance variations, leading to higher similarity at the level of protein biosynthesis between both tissues.

CONCLUSIONS: We show that tissue-specificity in rhythmic gene expression extends to the translatome and contributes to define the identities, the phases and the expression levels of rhythmic protein biosynthesis. Moreover, translational compensation of transcript abundance divergence leads to overall higher similarity at the level of protein production across organs. The unique resources provided through our study will serve to address fundamental questions of post-transcriptional control and differential gene expression *in vivo*.

Keywords: circadian clocks, translation, ribosome profiling, kidney, liver

Background

Circadian clocks serve organisms to synchronize behaviour, physiology and gene expression according to time of day. The mammalian circadian system consists of a master clock in the brain's suprachiasmatic nuclei (SCN) that receives photic inputs from the retina and synchronizes peripheral clocks present in most cells throughout the body. The molecular timekeeping mechanism – the core clock – consists of a network of transcriptional activators and repressors interacting in negative feedback loops (reviewed in [1, 2]). In the core loop, the heterodimeric transcription factor ARNTL:CLOCK (also known as BMAL1:CLOCK) drives the expression of its own repressors, encoded by the *Period (Per1, Per2, Per3)* and *Cryptochrome (Cry1, Cry2)* genes – a configuration also known as the positive and negative limbs of the oscillator. Additional feedback – in particular an interconnecting limb involving nuclear receptors of the REV-ERB (encoded by genes *Nr1d1, Nr1d2*) and ROR *(Rora, Rorb, Rorc)* family – intersects with the core loop, and numerous post-translational modifications of clock proteins further add to the complexity of the circuitry. The final outcome is a set of robustly cycling transcriptional activities peaking at different phases around the day that drive the rhythmic expression of hundreds to thousands of other genes, termed the clock output or clock-controlled genes (CCGs). It is noteworthy that, despite the probably (near-)identical molecular makeup of the core clock across cell types, CCGs show considerable tissue-specificity [3]. The co-regulation by core clock and tissue-specific (non-rhythmic) transcription factors may engender such cell type-specific rhythmic expression patterns, as shown to occur in *Drosophila* [4]. Overall, however, the origins of tissue-specificity in rhythmic gene output (and even in certain core clock parameters [5]) are poorly understood. Mechanisms that act at the post-transcriptional level and that impact daily mRNA and protein accumulation kinetics are plausible players in the generation of cell type differences as well.

Rhythmic gene expression has been mainly investigated at the transcriptome level i.e., using mRNA abundances as a primary readout. However, comparison of mRNA levels with datasets of genome-wide transcriptional activity and of protein abundances that have become available recently, has suggested that a surprisingly large fraction of gene expression oscillations may have post-transcriptional origins (reviewed in [6]). The many cases of protein rhythms that are independent of an underlying oscillating transcript (initially reported in a low-throughput mass-

63 spectrometric study from mouse liver already 10 years ago [7] and recently confirmed at a
64 comprehensive scale [8, 9]) point to important roles for translation, protein degradation and
65 protein secretion in shaping time of day-dependent proteomes. We [10] and others [11] have
66 recently used ribosome profiling, a genome-wide method that assesses translation efficiency
67 through the deep sequencing of ribosome-protected mRNA fragments, to chart the contribution of
68 translational control to daily protein biosynthesis in mouse liver. One conclusion that emerged
69 from the identified cases of translationally generated oscillations was that circadian clock activity
70 and feeding rhythms both contribute to regulating rhythmic gene expression outputs [10, 11].
71 Notably, the most abundant group of transcripts subject to rhythmic translation, i.e. mRNAs
72 encoding ribosomal proteins and other components of the translation machinery that all contain
73 5′-terminal oligopyrimidine tract (5′-TOP) sequences regulated by the mammalian target of
74 rapamycin (mTOR) [12], appear to be under the dominant control of feeding [11].
75 We have now performed ribosome profiling using a second organ from the same cohort of
76 animals, the kidney, which is an emerging circadian model organ with distinct rhythmic functions
77 [13]. By contrasting kidney and liver datasets we comprehensively assessed commonalities and
78 differences in their translatomes, and we evaluated in how far the regulation of translation
79 efficiency contributed to tissue specificity in rhythmic and constitutive protein biosynthesis.

80 Results

81 Around-the-clock ribosome profiling datasets from two organs

82 For our recent study of the liver translatome around-the-clock [10] we had used ribosome profiling
83 [14] (RPF-seq) on a time series of organs collected from mice sacrificed every 2 hours over the
84 24-hour day (12 timepoints in duplicate; Figure 1A). To generate a complementary dataset from a
85 second organ we chose the kidneys from the same cohort of animals. Liver and kidney express
86 thousands of genes in common [3, 15], thus providing a particularly suitable setting for a cross-
87 organ comparison of gene expression.
88 Applying the same experimental and computational methods as for liver RPF-seq [10, 16], we
89 obtained comparable high-quality data for kidney (see Supplementary Table S1 and Figure S1A-
90 C for details on sequencing and mapping outcomes). Briefly, ribosome footprints from both

organs showed similar enrichment for protein coding sequences (CDS) of mRNAs and depletion of untranslated regions (UTRs) (Figure 1B). Like the footprints from liver, also those from kidney exhibited excellent reading frame preference, which allowed resolving the 3-nt periodicity of coding sequences transcriptome-wide (Figures 1C and S2A-B). Moreover, the high correlation coefficients seen across replicates of the kidney time series for both RNA- and RPF-seq data indicated excellent biological and technical reproducibility (Figure S3A-B). We also used a recently developed tool, termed Ribo-seq Unit Step Transformation (RUST) [17], to confirm high technical similarity of datasets between organs (Figure S2C-D). Finally, principal component (PC) analysis on all available datasets (96 libraries, i.e. RPF-seq and RNA-seq from 2 organs, 12 timepoints, in duplicate) segregated the data according to the main experimental and biological covariates. PC1 (explaining 64.2% of variation) thus separated libraries according to organ, indicating that tissue origin represented the major source of divergence, followed by PC2 (28.4%) that separated RNA-seq (mRNA abundance) and RPF-seq (footprints/translation) (Figure 1D). The cyclic nature of the data was resolved in the representation PC3 vs. PC5 (together 12.5%), in which timepoints assembled to a near-perfect clock (Figure 1E). The larger circular arrangement of the liver vs. kidney time series suggested that rhythmic gene expression from liver contributed more strongly to overall variation than did kidney rhythms. This observation is in line with the notion that there are more, and higher amplitude rhythms in liver than in kidney [3]. Taken together, we concluded that the kidney data were of similarly high quality as our previous liver datasets [10]. Together, they would be suitable for comparative analyses of time of day-dependent and constitutive translation across two tissues.

Cross-organ differences in translation efficiency are widespread, of moderate scale, and partially compensate RNA abundance differences

To what extent do differences in translation efficiency contribute to different gene expression outputs across organs? We addressed this question using the set of 10289 genes whose expression was detectable in kidney and in liver at both RPF and RNA level (Figure 2A). From the ratio of CDS-mapping normalised read counts for RPF-seq relative to RNA-seq we first calculated relative translation efficiencies (TEs) per transcript and for each organ. TEs were overall rather

119 similar between tissues, with 95% of genes falling into a less than 3-fold range for the kidney/liver
120 TE ratio, as compared to a greater than 100-fold range for the transcript abundance ratio (Figure
121 2B). This observation was coherent with the considerably broader spread of mRNA abundances
122 vs. TEs across genes within each organ (greater than 500-fold vs. just over 10-fold, respectively;
123 Figure S5A-B) and is in line with a dominant role for the regulation of mRNA levels (i.e.,
124 transcription and mRNA decay) in controlling quantitative differences in gene output.
125 Intuitively, we had expected that RNA levels that were widely dissimilar between kidney and liver
126 and subsequently further modulated by organ-specific TEs, would probably give rise to even
127 greater cross-organ divergence at the RPF level. Intriguingly, however, the global correlation
128 between kidney and liver was better for footprint abundances than for transcript abundances
129 (Spearman ρ [RPF]: mean 0.784 vs. ρ [RNA]: mean 0.736; $p<2.2e-16$) (Figure 2C; Figure S3C-
130 D). This phenomenon was observed irrespective of whether the genes expressed only one
131 dominant protein-coding transcript isoform ("single isoform genes" in the following) that was
132 common to both organs, or whether they gave rise to different (including tissue-specific) mRNA
133 variants ("multiple isoform genes") (Figure 2D). The observed higher cross-organ concordance of
134 RPFs could have simply had technical reasons, for example if the RPF-seq protocol gave more
135 reproducible results than the RNA-seq protocol. We addressed this caveat by comparing
136 measurement errors (MEs) for RNA and RPF data using a similar approach as in a recent
137 publication [18]. We found that MEs scaled inversely with expression levels, as expected, and
138 showed some variation due to organ (Figure S6A,B,F,G). Especially in liver and among low
139 expressed transcripts, a tendency towards smaller MEs for RPF than for RNA was indeed visible
140 (differences statistically non-significant). In most other cases, however, measurement errors were
141 (in part significantly) higher for the transcripts' RPF counts than for their RNA counts. Of note, the
142 better cross-organ correlation of RPF vs. RNA levels seen in the full transcript set (Figure 2C)
143 was also evident within various transcript subsets (Figure S6C-E, H-L), including such subsets for
144 which RPF MEs were higher than RNA MEs (Figure S6E, L). It is thus unlikely that technical bias
145 was the reason for the higher RPF correlation. Finally, an analysis that we performed on
146 independent ribosome profiling datasets from rat liver and heart [19] allowed us to confirm the
147 phenomenon of higher concordance of RPF vs. RNA abundance also between these organs

148 (Figure S7A-C). Taken together, these findings are suggestive of a potentially broader biological
149 phenomenon that consists in the partial compensation of differences in a gene's mRNA
150 expression through counteracting effects exerted through its TE, resulting in the convergence at
151 the level of protein biosynthetic output (footprints, RPF) across tissues.

152 **Transcript features associated with cross-organ differences in translation efficiency**

153 Do particular transcript features have predictive value for organ-specific differences in translation
154 efficiency? To investigate this question we selected the genes with significantly different TEs
155 between tissues (N=5013; Wilcoxon signed rank test; FDR<0.01) and implemented a 1.5-fold cut-
156 off on TE ratio between the organs to retrieve the most pronounced cases (N=960) (Figure 2E;
157 Supplementary Table S2). Of these, 533 represented "single isoform genes" with no (or negligible
158 amounts of) expression of tissue-specific mRNA variants. For these genes, we examined whether
159 a higher TE in kidney (N=193) or in liver (N=340) was associated with specific transcript
160 characteristics. Of several features tested, we found that CDS and transcript lengths showed the
161 most significant association with differential TE (Figure S8A-B). Of note, we had previously seen
162 in liver that shorter coding sequences – i.e., transcripts encoding smaller proteins – are more
163 efficiently translated [10]. Our present analyses suggest that such transcripts are also more prone
164 to tissue-specific regulation at the translational level. Other sequence features showed some bias
165 within the differential TE gene sets as well, although the effects were overall weaker and less
166 consistent. Briefly, the 5′ UTRs of genes with higher TEs in liver were longer and predicted to fold
167 more strongly. By contrast, transcripts with higher kidney TEs were associated with lower 5′ UTR
168 GC content and slightly shorter 3′ UTRs. No association with differential TE was found for the
169 Kozak sequence context score.

170 We also investigated two functional classes of sequence features, miRNA binding sites and
171 upstream open reading frames (uORFs), for association with differential TE. Of note, the 960 "TE
172 different" transcripts were not enriched for any predicted miRNA binding sites, making it unlikely
173 that this class of post-transcriptional regulators is a major player in establishing tissue-specific
174 TEs (data not shown). We had previously observed that in the liver the presence of a translated
175 uORF in the 5′ UTR was strongly predictive of low TE at the main ORF [10]. An analogous

176 relationship was evident in kidney as well (Figure S5C). To assess whether uORF translation was
177 associated with TE differences across organs, we compared how the identified uORF-containing
178 transcripts (i.e., single isoform genes showing translated uORFs in at least one organ; N=1377)
179 distributed to the differential vs. non-differential TE gene sets. The group of genes with higher TE
180 in liver was significantly enriched for transcripts with translated uORFs (p=6.08e-04; Fisher's
181 exact test) and there was slight depletion among genes with higher TE in kidney (not significant)
182 (Figure S8C). Only few differential TE genes exhibited uORF translation that was exclusive to one
183 organ, but there was a tendency for kidney-specific translation of uORFs to be associated with
184 higher TE on the CDS in liver, and vice versa (Figure S8D). For the genes with uORFs translated
185 in both tissues, we expected that cross-organ differences in the strength of uORF usage would
186 negatively correlate with TE differences at the CDS. However, such a trend was only visible for
187 liver differential TE genes (Figure S8E), and globally, uORF and CDS TEs even showed slightly
188 positive correlation. In summary, these analyses suggested that uORF translation contributed to
189 some extent (and especially for genes that were more efficiently translated in the liver) to cross-
190 organ differences in TE; however, the overall impact appeared limited (see Discussion).
191 We next included the "multiple isoform genes" in the analyses and asked whether transcript
192 isoform diversity between the two organs – i.e., the occurrence of tissue-specific mRNA variants
193 generated by alternative transcriptional start sites, splicing, and 3′ processing – had any
194 relationship to differential TE. Briefly, using our RNA-seq data we first compiled an inventory of all
195 annotated, protein-coding transcript isoforms and their estimated relative expression levels per
196 gene and tissue. We then used the Hellinger distance [20] as a measure of dissimilarity in isoform
197 expression levels between kidney and liver. A value of 0 for this metric indicates that a gene has
198 identical isoform distribution in both tissues (i.e., these are essentially the "single isoform genes"
199 described above), while a value of 1 denotes a lack of overlap in expressed isoforms. Globally,
200 the 960 genes with differential TE showed significantly higher Hellinger distances than the
201 remainder of the expressed genes (p=3.74e-04; Kolmogorov-Smirnov-test) (Figure 2F).
202 Molecularly, the term "transcript isoform" comprises variations affecting 5′ UTR, CDS, and 3′ UTR.
203 By comparing the genes for which all expressed variants affected exclusively one single feature,
204 or for which this particular feature was not affected at all, it became apparent that transcript

205 diversity in the 5′ UTR was particularly strongly associated with differential TE (Figure 2G). By
206 contrast, variation in the CDS showed significantly less association with cross-organ differences
207 in translation efficiency (Figure S9A-B). Although the low number of available transcripts bearing
208 exclusively 3′ UTR differences precluded a rigorous interpretation, 3′ UTR variation did not appear
209 to be associated with differential TE either (Figure S9C). Altogether, we thus concluded that TE
210 differences between tissues may, at least in part, have their origin in tissue-specific transcript
211 variants, especially through alternative 5′ UTRs.
212 Finally, we were interested in whether cross-organ differences in translation efficiency affected
213 specific pathways. For the 640 "TE different" genes that showed increased TE in liver (Figure 2D),
214 gene ontology (GO) analyses revealed significant enrichment for categories related to
215 transcription (Supplementary Table S2). Conceivably, tissue-specific translational control of
216 transcriptional regulators may thus impact also on the organs' transcriptomes. The 320 "TE
217 different" genes that were translated better in kidney did not show any significant enrichment.

218 **Translational modulation of phase of oscillation in kidney**

219 We next turned to the analysis of factor time across the datasets. We annotated rhythmic events
220 in kidney with the same methodology as previously for liver, including a 1.5-fold cut-off on peak-
221 to-trough amplitudes [10]. A list of the detected RNA and RPF rhythms and genome-wide gene
222 expression plots are provided in Supplementary Table S3 and Supplementary Dataset S1,
223 respectively. Our analyses yielded 1338 and 977 genes that cycled at the RNA abundance and
224 footprint level, respectively, with an overlap of 542 genes (Figure 3A). As discussed later, this
225 relatively modest overlap (542 genes corresponds to 41% and 55% of all "RNA rhythmic" and
226 "footprints rhythmic" cases, respectively) likely underestimates the full extent of shared rhythmicity
227 and only contains the most robustly oscillating gene expression events, which we further explored
228 in the following.
229 Interestingly, the analysis of rhythmicity parameters across the 542 genes revealed that the timing
230 of their RPF peaks relative to their RNA peaks had a significantly different and broader
231 distribution than the corresponding set from liver ($p<1.0e-04$; permutation test) (Figure 3B). This
232 observation suggested that the phase of protein biosynthesis rhythms was subject to marked

translational modulation in kidney. In liver, by contrast, RPF peaks were more tightly gated by RNA abundance peaks. Surprisingly, maximal translation tended to *precede* maximal RNA abundance in kidney (Figure S10A), as globally the mean RPF peak phase was advanced (-0.123 hours) and also RPF rhythms were enriched for phase advances (282) vs. delays (260), albeit neither reaching statistical significance (p=0.16, Wilcoxon rank sum test).

The above analyses used different rhythmic gene sets for kidney than for liver, potentially compromising comparability. The observed differences in the RPF-RNA phase relationships could thus have simply arisen from transcript-specific rather than from tissue-specific differences in the timing of translation. We thus analysed the group of 178 genes whose RNA and RPF profiles were rhythmic in both organs (Figure 3C; Supplementary Table S4; Supplementary Dataset S2). Again, the distribution of RPF-RNA offsets was significantly broader in kidney than in liver (Figure 3D; p=0.007, permutation test) with an RPF peak phase advance in kidney (mean -0.143 h) and a phase delay in liver (mean 0.036 h) (Figure S10B-C). We next calculated the gene-wise RPF-RNA peak phase difference in kidney relative to that in liver. More genes showed their RPF maxima earlier (96) than later (82) in kidney vs. liver, with a mean advance of -0.178 h (Figure S10D), but again without passing statistical significance (p=0.152, Wilcoxon rank sum test).

Conceivably, we lost statistical power and introduced error in the above analyses by restricting the phase comparisons merely to the peaks of the rhythmic curve fits. We thus sought a method that would take into account phase differences between RPF and RNA profiles over all data points. To this end, we used cross-correlation to quantify the similarity between the RPF and RNA time series as a function of sliding one series on the time axis relative to the other. When the time series were not shifted against each other at all (RPF-RNA lag = 0 h), the RPF-RNA cross-correlation values were overall highest, as expected, and they were significantly higher in liver, in line with stronger gating of RPF rhythms relative to RNA oscillations in this organ (Figure 3E). Importantly, when cross-correlation of RNA was calculated with earlier RPF time points (negative RPF-RNA lags; see in particular lags of -2 h to -8 h in Figure 3E), kidneys scored significantly higher than livers. Sliding the series in the other direction, however, rather led to overall better correlations in the liver (see lags of +4 to +8 in Figure 3E; liver-kidney difference non-significant).

261 Taken together, these analyses underscored that there was asymmetry in the data with RPF
262 rhythms preceding RNA rhythms specifically in the kidney.
263 We confirmed kidney-specific translational phase advances by visual inspection of individual gene
264 expression profiles. Figure 3F shows the profiles for the genes *Hlf, Nampt, Slc5a6*, *Tardbp*,
265 *Dnajb4*, *Cgn* and *Etnk2*, which all show an RPF phase advance of up to several hours relative to
266 RNA. Cross-correlation analysis for the individual genes confirmed kidney-specific, phase-
267 advanced translation as well (Figure 3G).
268 At first sight, translation that is phase-advanced to mRNA abundance is counterintuitive.
269 Conceivably, it may occur when translation efficiency is not constant, but decreases over the
270 lifetime of an mRNA. TEs may be higher on freshly synthesised messages that have long poly(A)
271 tails, and decrease as a result of gradual deadenylation even before transcript stability and
272 abundance are affected as well [21]. In keeping with the hypothesis of cross-organ differences in
273 poly(A) kinetics, we have observed that most subunits of the major cytoplasmic deadenylase
274 complex, CCR4-NOT, are significantly more highly expressed in kidney than in liver (Figure
275 S11A-C). Higher deadenylase activity in kidney could provide an attractive molecular explanation
276 for the observed tissue-specific differences in RPF-RNA phasing, and for RPF rhythms that are
277 phase-advanced to RNA oscillations.

278 **High tissue divergence in translationally driven rhythms**

279 Rhythmicity detection algorithms are sensitive to false-negatives i.e., to classify gene expression
280 profiles as “non-rhythmic” (for example because they fail imposed thresholds on amplitude or
281 FDR) although the underlying temporal patterns may still be more similar to, and more likely to
282 be, rhythmic than invariable. Of note, the lack of canonical methods to reliably determine true
283 absence of rhythms is a common problem in the field (see recent review by [6] for discussion).
284 Venn diagrams that simply overlap rhythmic gene sets hence need to be interpreted with caution.
285 For these reasons, the extent of “RNA only” and of “footprints only” oscillations in Figure 3A is
286 likely not reported reliably and subject to overestimation. The heatmaps of the corresponding
287 RNA and RPF profiles support this notion as well (Figure S12B, D).

288 In order to identify the true-positive “translation only” cycling transcripts with higher reliability, we
289 implemented the same methodology as in our previous study [10]. Briefly, we used the analytical
290 framework *Babel* [22] to preselect all transcripts whose translation efficiency changed significantly
291 over the day (and/or whose TEs deviated significantly from the global transcript population).
292 Rhythmicity analyses were then performed on this gene subset and yielded 92 cases with the
293 sought-after temporal profiles of rhythmic translation on non-rhythmic mRNAs (Figure 4A).
294 Comparison with the 142 genes of the analogous set from liver revealed near-perfect tissue
295 specificity of translationally driven oscillations. Only two genes, *Abcd4* and *Lypla2*, were shared
296 between the organs; they were both among the least compelling cases of “translation only
297 rhythms” that our method had identified, as judged by visual inspection (Figure 4B).
298 Interestingly, not only the identity of rhythmically translated genes, but also the time-of-day at
299 which the majority of rhythmic translation events occurred, was highly tissue-specific. The phase
300 histograms thus showed striking differences in the peak time distributions between the organs
301 (Figure 4C-D; difference in distributions: p=1.66e-04; W = 17.403, df = 2; Watson-Wheeler test for
302 homogeneity of angles). Of note, the enrichment for translational maxima at the light-dark
303 transition (*Zeitgeber* time, ZT10-16; ZT00 corresponds to lights-on and ZT12 to lights-off) that
304 dominated the distribution in liver (Figure 4D, F) was virtually absent from kidney (Figure 4C, E).
305 Instead, kidney showed enrichment for transcripts with maximal translation occurring around ZT4
306 and ZT16. Visual inspection of individual examples confirmed the organ specificity of RPF
307 rhythms. The cases of robust translational oscillations that we [10] and others [11, 12] had
308 previously identified in liver were thus absent or severely blunted in kidney. This included mRNAs
309 encoding ribosomal proteins (RPs), which make up the bulk of genes showing a translational
310 surge at the light-dark transition (e.g. *Rps25*, *Rpl23a*), as well as transcripts encoding the
311 transcription factors *Deaf1* (deformed epidermal autoregulatory factor 1) and *Mxi1* (MAX
312 interactor 1), and mRNAs containing iron-responsive elements in their 5′ UTRs (e.g. Ferritin light
313 chain 1, *Ftl1*) (Figure 4G), all of which we had previously reported as translationally rhythmic in
314 liver [10]. Rhythmic translation exclusive to kidney was not significantly enriched for particular
315 pathways (data not shown), and the temporal profiles were overall of lower amplitude than those
316 seen for liver; *Tma7* (Translational machinery associated 7 homolog), *Ddb2* (Damage-specific

317 DNA binding protein 2), *Actg1* (Actin, gamma, cytoplasmic 1) and *Hoxd3* (Homeobox D3; not
318 expressed in liver) were among the most distinct examples (Figure 4H).
319 In summary, we concluded that temporal changes in TE were strikingly tissue-specific and overall
320 relatively rare in kidney. Specifically for transcripts encoding RPs and other components of the
321 translation machinery, which are the most prominent group of TE rhythmic genes in liver, it has
322 been suggested that feeding-dependent mTOR-signaling underlies the translational upsurge at
323 the light-dark transition via a mechanism involving the 5′-terminal oligopyrimidine (5′-TOP) motifs
324 that these transcripts carry [11, 12]. Interestingly, the TE comparison between both tissues
325 revealed that kidney RP translation occurred at a relatively high level throughout the day (Figure
326 4I). The lack in rhythmicity for RP genes in this organ may thus result from an absence of
327 translational repression during the light phase rather than a lack in activation in the dark phase. It
328 may indicate that the kidney is less sensitive to systemic cues engendered by feeding and fasting
329 (see Discussion).

330 **Different degrees of tissue specificity in core clock gene expression at the level of RNA**
331 **abundance and protein biosynthesis**
332 Clocks exhibit functional differences across cell types and organs, for example at the level of
333 rhythmicity parameters (e.g. free-running period and phase [5]), of clock output gene repertoires
334 [3], of oscillator strength and robustness [23, 24], or with regard to clock gene loss-of-function
335 phenotypes [25]. Conceivably, the precise timing and level at which the various clock proteins are
336 produced may modulate properties of the clock circuitry and underlie some of the
337 abovementioned functional variations. In order to investigate these possibilities we compared the
338 expression of core clock components in both organs.
339 We first investigated transcript and footprint RPKMs as averages over timepoints to assess the
340 cumulative daily production of clock RNAs and proteins. Most core clock genes showed a
341 considerable degree of organ-specificity in their expression levels that was readily appreciable in
342 the footprint vs. transcript abundance representation with both organs overlaid in a single graph
343 (Figure 5A). Two tissue differences caught our particular attention. First, the balance between the
344 transcriptional activators *Rora/Rorc* and repressors *Nr1d1/Nr1d2* differed markedly between

345 organs and was skewed towards repression in kidney (i.e., higher *Nr1d1/2* and lower *Rora/c*
346 RPKMs in kidney, Figure 5A-B). These transcriptional regulators bind to shared sequence
347 elements on DNA and form the "interconnecting limb" within the rhythm-generating clock circuitry.
348 In addition, they also control an output branch of the oscillator [1, 2]. It is hence conceivable that
349 adjusting the relative levels of NR1D1/2 vs. RORs tailors clock-controlled gene expression in a
350 tissue-specific fashion. Our observation of an active state of this output branch in liver and a more
351 repressed state in kidney, is fully consistent with the current knowledge of its target genes and
352 knockout phenotypes, which point to a prominent role in the regulation of hepatic pathways such
353 as lipid, cholesterol and bile acid metabolism [26].
354 A second tissue difference concerned the main constituents of the negative limb, the Period (*Per*)
355 and Cryptochrome (*Cry*) genes. Heterotypic PER:CRY protein complexes inhibit ARNTL:CLOCK-
356 driven transcriptional activity and thus lie at the core of the oscillator's principal negative feedback
357 loop. We observed a shift to more PER (and slightly less CRY) biosynthesis in kidney (Figure 5B).
358 PERs (and in particular PER2) are considered stoichiometrically rate-limiting components of the
359 PER:CRY complex, and increased PER2 dosage engenders long periods [27, 28]. Interestingly,
360 tissue explant experiments have shown that kidney clocks free-run with almost 1.5 hour longer
361 periods than liver clocks [5], as would be predicted from the increased PER biosynthesis that our
362 analyses revealed. As a more general concept, we deem it conceivable that the modulation of
363 biosynthesis levels for individual clock proteins may be a more general mechanism to engender
364 distinct differences in clock parameters across cell types.
365 We noted that for the majority of clock genes (*Npas2, Cry1, Cry2, Per1, Per2, Per3, Nr1d1, Rorc)*
366 the tissue differences were less pronounced at the RPF than at the RNA level (Figure 5B),
367 indicating that translation efficiencies partially counteracted RNA expression differences. Only in
368 four cases (*Clock, Arntl, Nr1d2, Rora*) TEs exacerbated transcript abundance differences and led
369 to higher tissue differences at the RPF level. Interestingly, this observation could also be made in
370 the time-resolved data. As a measure of similarity between rhythmic profiles, we used the
371 Euclidean distances calculated between the four rhythmic traces of each individual gene (i.e.,
372 RNA and RPF in kidney and liver; Figure S13). Hierarchical clustering of the similarities for the
373 ensemble of the 12 main core clock genes showed that RPF rhythms from the two organs

374 grouped together (Figure 5C). Clock protein biosynthesis rhythms between organs were thus
375 more similar than RNA and RPF rhythms within organs. By contrast, the 178 common rhythmic
376 genes identified in Figure 3C – serving as a control set for this analysis – revealed within-organ
377 clustering (Figure 5D). These findings underscored that translational compensation was occurring
378 within the core clock, where it led to more similar rhythms in clock protein biosynthesis than would
379 have been predicted from the rhythmic RNA abundance profiles. This phenomenon was,
380 however, not a general feature of all rhythmic gene expression.
381 The transcriptome-wide analyses described further above had shown only weak signs of
382 association between cross-organ differences in TE and in uORF usage (Figure S8C-E). However,
383 we knew from our previous work in liver that at least five core clock transcripts (*Nr1d1, Nr1d2,*
384 *Cry1, Clock, Arntl)* contained translated, potentially regulatory, AUG-initiated uORFs [10]. We
385 therefore examined whether for any of these concrete cases there was evidence for a connection
386 between uORF translation and cross-organ TE differences. The read distribution along the
387 transcripts (Figure S14A) and the marked frame preference of RPF reads (Figure S14B)
388 confirmed that the footprints mapping to our annotated uORFs likely reflected active translation.
389 However, only in one case, *Nr1d2*, there was a distinct anticorrelation between uORF usage and
390 TE differences on the CDS (Figure 5E). *Nr1d2* contains two translated uORFs in the 5′ UTR
391 (Figure 5F), whose decreased usage in kidney was accompanied with higher TE on the CDS in
392 this organ (Figure 5E). For *Nr1d2*, differential uORF usage could thus represent a plausible
393 mechanism that contributes to regulating organ-specific gene expression output at the
394 translational level, keeping NR1D2 biosynthesis low in liver and high in kidney.

395 Discussion

396 Given that the functionally relevant output of most gene expression is the protein, quantitative and
397 genome-wide analyses of protein biosynthesis are of high interest to complement the wealth of
398 transcriptomics data that is already available. Of note, only the fairly recent development of the
399 ribosome profiling technique [29] has made it possible to analyse translational events in a
400 quantitative, high-throughput fashion. Our study of two paradigms of differential gene expression,
401 i.e. its tissue- and its time of day-dependence, is among the first of its kind and, together with the

402 associated datasets and resources, will likely be of wide interest and utility to researchers working
403 in the chronobiology and gene expression fields.
404 We have addressed several, rather fundamental questions that go beyond the chronobiological
405 focus of the study: How does the dynamic range of translation efficiency compare to that of
406 transcript abundances across two distinct organs of an animal? Is translation efficiency a default
407 transcript property and comparable across two tissues, or do TEs become reinterpreted
408 depending on cell type or organ? Does cross-tissue variability of TEs come with any direction i.e.,
409 is there a global tendency to either reinforce or to counteract transcriptomal differences?
410 To our knowledge, only one previous study has reported on ribosome profiling datasets from two
411 complementary mammalian tissues, rat liver and heart [19]. This study also included animals with
412 different genetic backgrounds as covariates in the experimental design, and its main focus was
413 on strain differences in translation rather than on tissue differences. Our analyses based on more
414 than 10000 genes commonly expressed in liver and kidney show that cross-organ TE differences
415 are widespread, but of limited magnitude. Across genes in a tissue and for individual genes
416 between tissues, the dynamic range of translation efficiencies is thus about 30-50-fold narrower
417 than that of transcript abundances. These findings are coherent with the view that major
418 differences in gene expression are set up at the level of transcription (possibly with some
419 influence coming from RNA stability as well), whereas differences in translation rate have more of
420 a modulatory role. It is intriguing that this modulation is overall characterised by directionality, with
421 TE differences between tissues globally counteracting some of the mRNA abundance differences.
422 Such translational compensation has previously been observed for divergent transcript
423 expression levels across yeast species [30] and across different rat strains [19]; our study now
424 extends this observation to gene expression across organs. Moreover, the idea of translational
425 compensation is conceptually similar to findings that proteomes are evolutionarily more highly
426 conserved than transcriptomes [31, 32]. As an underlying common principle, these cases may
427 indicate that selective pressure on precise gene expression levels likely acts on protein
428 abundances, whereas a certain degree of variability (even noise) in RNA levels may be tolerated
429 without further consequences. It will be exciting to study the underpinnings of translational
430 compensation further, across tissues and across species.

431 Maybe not unexpectedly, there was no dominant, distinct sequence feature that could serve as a
432 predictor for cross-organ TE differences. Rather, we found several associations with a number of
433 transcript characteristics. Conceivably, these contribute collectively to modulating TEs in concert
434 with the specific cellular and tissue environment and possible cell type differences in the
435 translation machinery including its regulators and trans-acting factors. While our ribosome
436 profiling studies have allowed us to record the outcome of such regulation at high resolution,
437 understanding its causes represents an exciting challenge for the future. For now, we can only
438 infer that an overarching theme of the identified associations is a connection to 5′ UTRs, which is
439 in also in line with the notion that initiation is rate-limiting for most translation events. We thus
440 observed associations of cross-organ TE differences with 5′ UTR length, with uORF usage, with
441 GC content and folding potential, as well as with transcript isoform diversity that affected the 5′
442 UTR. We would like to point out that comprehensive uORF annotations remain a bioinformatics
443 challenge that is far from resolved. We have therefore restricted our analyses to AUG-initiated
444 ORFs, inevitably leading to a bias towards false-negatives in uORF annotation. As we will learn
445 how to annotate uORFs more comprehensively and more precisely in the future, it may be worth
446 revisiting the relationship between differential TE and uORF translation in our datasets in order to
447 evaluate whether a clearer role for these regulatory sequence elements will emerge.
448 Our study has led to novel insights into rhythmic gene expression. The extent to which rhythmicity
449 is generated by the temporal regulation of translation has been the subject of speculation ever
450 since the first report of rhythmic proteins encoded by non-rhythmic mRNAs [7]. Our kidney
451 datasets complement recent time-resolved ribosome profiling data from liver [10, 11] and from a
452 cell line [33]. As compared to liver, the number of transcripts subject to translational rhythms in
453 kidney is slightly lower, but overall in a similar order of magnitude with around 1% of the
454 transcriptome affected. It came as a surprise that translational rhythms were essentially tissue-
455 specific in terms of the affected genes and the phase distributions. A possible explanation could
456 be that these rhythms are driven by rhythmic systemic cues to which tissues do not respond
457 equally. The effects of feeding and mTOR signalling, for example, may be more pronounced in
458 liver due to the dedicated role that this organ plays in energy homeostasis and fasting responses,
459 thus explaining the differences in translational oscillations for RP genes. Beyond the role that

460 translation has in generating rhythms, our analyses have pointed to an additional, rhythmicity-
461 modulating role that appears to affect gene expression quite broadly, i.e. the timing of the phase
462 of protein biosynthesis oscillations relative to that of mRNA abundance rhythms. Consistent with
463 work by the Green lab that showed interactions between polyadenylation status of mRNAs and
464 rhythmic protein expression in the liver [21], it is tempting to speculate that related mechanisms
465 are operative across organs, with tissue-specific deadenylation kinetics tuning the timing of
466 rhythmic protein biosynthesis. Finally, our study is a first attempt to resolve tissue differences in
467 core clock gene expression as a factor contributing to functional differences of the oscillator. It is
468 interesting that the core clock mechanism has a long-standing history of being referred to as a
469 "transcription-translation feedback loop" [34], although the actual feedback occurs at the
470 transcriptional level, and possible mechanistic functions of translational regulation have not been
471 much investigated. Our cross-organ comparison of core clock protein biosynthesis suggests that
472 translational control – including through the activity of uORFs [10, 33] – is of regulatory interest
473 and represents a way by which the identical set of core clock genes could form circuitries with
474 different stoichiometry of its main components. As a result, both clock parameters and output
475 gene repertoires may be organ-specifically tuned.

476 Conclusions

477 How translational differences contribute to overall gene expression diversity is still poorly
478 understood. Our study uncovered translational changes that occur across two paradigms of
479 regulated gene expression, i.e. around-the-clock and between tissues. Daily gene expression
480 rhythms generated at the translational level were strongly organ-specific with regard to the
481 identities and phase distributions of affected genes. Moreover, our data indicate that translation
482 efficiency differences between organs can adjust the timing of protein production from rhythmic
483 mRNAs, and the levels of core clock protein production, in agreement with the tissue-specificities
484 observed in clock output gene sets and clock parameters. Together, these results are consistent
485 with an important role of post-transcriptional mechanisms in mammalian circadian gene
486 expression regulation. Beyond the temporal dimension, we have explored constitutive protein
487 biosynthesis across organs. Our quantitative analyses underscore that gene expression

488 divergence is largely programmed at the transcript abundance level. Interestingly, the widespread
489 differences in translational efficiency that we detected between organs even serve to achieve
490 higher concordance in protein production between tissues. Conceivably, such translational
491 compensation reflects a selective pressure to maintain precise protein levels rather than mRNA
492 levels. The high-resolution genome-wide translatome datasets generated in this study will allow
493 further explorations into the mechanisms of post-transcriptional control and differential gene
494 expression *in vivo*.

495 Methods

496 Animals

497 12-week old male mice (C57BL/6J; Janvier Labs) were entrained for two weeks to light:dark
498 12:12 cycles with *ad libitum* access to food and water and were anesthetized (isoflurane) and
499 sacrificed every two hours (ZT0 - ZT22, with ZT0 corresponding to "lights-on") for two daily
500 cycles. Livers and kidneys were removed and processed either directly or flash-frozen in liquid
501 N_2. All experimental procedures were approved by the Veterinary Office of the Canton Vaud
502 (authorisation VD2376).

503 Ribosome profiling

504 Generation of liver RPF-seq and RNA-seq libraries using the ARTseq ribosome profiling kit
505 (Epicentre) was described recently [10, 16]. Kidney libraries were prepared in the same manner,
506 with a single modification to the order of steps in RPF library preparation. After RNase treatment
507 and recovery of ribosome-protected fragments, 5µg of material was first rRNA-depleted (Ribo-
508 Zero magnetic kit, Epicentre) and then purified by 15% PAGE. In the formerly prepared liver
509 libraries, Ribo-Zero treatment and PAGE purification had been inverted because at the time we
510 had found that changing the order had a beneficial effect on obtaining highly concentrated
511 libraries. For the kidney samples, however, we noted that this modified order led to higher
512 contamination with reverse-strand rRNA probes bleeding from the Ribo-Zero kit and we thus
513 reverted to ARTseq's original order. All other steps and materials were identical between liver and
514 kidney samples and followed the ARTseq ribosome profiling kit instructions. RPF and RNA
515 libraries were sequenced on an Illumina HiSeq 2500.

516 **Sequencing data processing, alignment and quantification**

517 Processing, quality assessment, alignment and quantification of sequencing data were performed
518 as described previously [10, 16]. Briefly, after adapter trimming using Cutadapt [35], the length
519 distribution of trimmed reads was used to assess the quality of nuclease digestion and size-
520 selection, which is particularly important for RPF libraries (Figure S1B). Trimmed reads were
521 filtered by size (26-35 nt for RPF; 21-60 nt for RNA) using an in-house Python script, and
522 sequentially mapped to mouse rRNA, human rRNA, mitochondrial tRNA, mouse tRNA, mouse
523 cDNA (Ensemble mouse database release 75) using Bowtie v2.2.1 [36] and mouse genome
524 (GRCm38.p2) using Tophat v2.0.11 [37]. Trimmed and filtered sequences were also directly
525 mapped against the mouse genome (Tophat v2.0.11) in order to estimate expressed transcript
526 models in each organ (using Cufflinks v2.2.1 [38]). Transcriptome-mapping reads in the
527 sequential alignment were counted towards their location into the 5′ UTR, CDS or 3′ UTR of the
528 transcript, based on feature annotation (Ensemble mouse release 75). Mappable and countable
529 feature lengths were not calculated for this study (see “faux reads analysis” in the “Quantification
530 of mRNA and ribosome footprint abundance” section of Supplemental Experimental Procedures
531 of previous study [10]) as its contribution was negligible for further analyses. Therefore RPKM
532 calculations in this study were not corrected with such factor. Read counts in RNA-seq and RPF-
533 seq datasets were normalised with upper quantile method of edgeR [39] and RPKM values were
534 calculated as the number of reads per 1000 bases per geometric mean of normalised read counts
535 per million. Relative translation efficiencies (TE) were calculated as the ratio of RPF-RPKM to
536 RNA-RPKM per gene per sample. Reading frame and nucleotide periodicity analyses were
537 performed as in [10]. Principal Component Analysis (PCA) relied on a combined matrix of CDS
538 counts for RPF and RNA from both liver and kidney and following the same approach as before
539 [10]. Ribo-seq Unit Step Transformation (RUST) analysis was used to assess whether the
540 sequencing libraries were globally of similar quality in terms of their local footprint densities [17].
541 RUST is a simple normalisation method that reduces the heterogeneous noise in the data and
542 allows identification of mRNA sequence features that affect footprint densities globally. We used
543 the version 1.2 of the published rust_codon.py standalone python script with minor modifications
544 to reflect the experimental settings as closely as possible (i.e., A-site offsetting). RUST codon

545 profile and corresponding Kullback–Leibler (K–L) divergence for each library (RPF and RNA) was
546 generated against a database of 8012 single protein isoform transcript sequences using all
547 mapped reads with a length of 28-32 nt. The K-L divergences from all samples for each
548 combination of tissue (kidney or liver) and read type (RPF or RNA) were used to generate K-L
549 profiles at the 0, 10, 25, 50, 75, 90, and 100th quantiles.

550 **Correlation analyses and assessment of translational compensation across organs**

551 Correlation of RNA-seq and RPF-seq across organs: Kidney vs. liver correlations at the levels of
552 RNA- and RPF-seq (i.e., Figure 2B; Figure S6C-E, H-L) were calculated in a pairwise fashion for
553 each of the 24 samples (12 timepoints, 2 replicates/timepoint), as livers and kidneys of each
554 replicate originated from the same animals. Significance of the difference in the Spearman
555 coefficients between both distributions was assessed by paired t-test on Fisher z-transformed
556 coefficients. Heart vs. liver correlation at the levels of RNA and RPF-seq (Figure S7A) was
557 calculated from the study [19], using the BN-Lx reference rat strain data. Since the five heart and
558 liver replicates in this study did not come from the same animals, we calculated all possible
559 pairwise correlation coefficients between heart and liver (i.e., 25), and compared all possible
560 combinations of 5 coefficients between RNA- and RPF-seq (paired t-test on Fisher z-transformed
561 coefficients).

562 Measurement error: Measurement errors (Figure S6A,B,F,G) were calculated similarly to [18]
563 using the meas.est() function from smatr R package [40]. Genes were first binned according to
564 average expression level (calculated as the fourth root of the product of liver RNA-seq, liver RPF-
565 seq, kidney RNA-seq and kidney RPF-seq) into 10 groups, each containing 10% of all genes.
566 Within each bin, the measurement error was calculated separately for RNA- and RPF-seq and for
567 liver and kidney, using the two replicates (log of normalised CDS counts) to estimate the error,
568 and the 12 timepoint samples to estimate its variability. For the analyses using a filtered gene set
569 (Figure S6F-G), genes that showed a mean expression ratio (either between organs or between
570 RNA- and RPF-seq) greater than 2 for all timepoints were excluded (9236 genes used in
571 analysis).

572 **Analyses of differential translation efficiency**

573 To test for differential translation efficiency (TE) between liver and kidney we used the Wilcoxon-
574 signed rank paired test, using all 24 samples (12 timepoints; 2 replicates/timepoint) as replicates;
575 resulting p-values were FDR-corrected. A gene was defined as having differential TE when FDR
576 < 0.01 and the inter-organ difference in TE was at least 1.5-fold (Figure 2E).
577 Analysis of transcript usage diversity across organs: For each gene g, P(g) = (p 1 ,...,p n) is the
578 vector of the relative expression proportions of its n protein-coding transcripts, as estimated from
579 our RNA-seq analysis (see Sequencing data processing, alignment and quantification). To
580 quantify the dissimilarity in relative transcript isoform expression between liver L and kidney K, the
581 Hellinger distance H is defined as:

$$H(P_L(g), P_K(g)) = 1/sqrt(2)\sqrt{\sum_{i=1}^{n}(\sqrt{p_L i} - \sqrt{p_K i})^2} \qquad (1)$$

582

583 In order to detect the transcript features that were associated with tissue specificity in TE, we
584 selected genes whose transcript diversity between both organs originated from, or was excluded
585 from, 5′ UTR, CDS, or 3′ UTR, based on feature annotation information for the detected protein-
586 coding transcripts (Figure 2G and Figure S9).
587 Study of transcript characteristics: For single-isoform genes, we investigated whether a particular
588 transcript characteristic (length, GC content, Kozak context, structure) could be predictive of
589 differential TE. Length and GC content were determined directly on the whole transcript and/or on
590 the region of interest (5′ UTR, CDS, 3′ UTR). Kozak context was scored according to the
591 consensus sequence GccA/Gcc**AUG**G, where upper-case letters denote highly conserved bases
592 (scored +3), lower-case letters indicate the most common nucleotides (scored +1), and bold is the
593 start codon (not scored), giving a maximum score of 13. Minimum free energy secondary
594 structures on the 5′ UTR were predicted with RNAfold from ViennaRNA package with default
595 parameters [41].

596 **Detection and translation efficiency calculation for uORFs**

597 To assess the impact of differential uORF usage on TE differences across organs, uORFs were
598 identified as in our previous study [10]. Briefly, genes expressing a single protein-coding isoform
599 in both organs were used for this analysis (N=5815). We selected uORFs with an AUG start

600 codon and a length of at least 18 nt to the first in-frame stop codon and considered them as
601 translated if the reads showed significant frame bias towards the reading frame of the uORF start
602 codon and if coverage was >10%. uORF translation efficiency was calculated from the ratio of
603 RPF-seq to RNA-seq reads whose predicted A-sites mapped to the annotated uORF regions. If
604 several uORFs partially of completely overlapped on a given 5′ UTR, a composite uORF was
605 considered for read counting. uORFs overlapping with the CDS in the same frame were not
606 considered. When they overlapped in different frames, only reads mapping to the 5′ UTR-specific
607 uORF sequence (but not the overlapping sequence) was considered for quantifications.

608 **Rhythmicity analyses**

609 Rhythmicity detection and rhythmic parameter estimations in each dataset (RNA-seq and RPF-
610 seq, liver and kidney) were done based on Akaike information criterion (AIC) model selection as
611 in our previous study [10]. The Babel computational framework [22] was used to detect
612 rhythmically translated genes from constantly expressed mRNAs within each organ. For cross-
613 correlation of time series to compare the daily profiles of rhythmic genes beyond their peak
614 differences, we used the ccf function in R. As we computed the correlations of the RPF-seq with
615 respect to the RNA-seq profiles, negative lag values correspond to RPF leading
616 RNA.

617 **Hierarchical clustering of rhythmic genes**

618 To evaluate the similarity of the expression profiles for rhythmic genes, a dissimilarity matrix was
619 computed for each gene of interest, based on the Euclidean distance between the RNA-seq and
620 RPF-seq expression profiles within and across organs. A hierarchical clustering tree was
621 constructed on the weighted average of the dissimilarity matrices of genes under consideration
622 (core clock genes in Figure 5C or all rhythmic genes in Figure 5D), using the “average” clustering
623 method. The R functions{packages} dist{stats}, fuse{analogue} and hclust{stats} were used for
624 computing the individual dissimilarity matrices, the weighted mean dissimilarity matrix, and the
625 hierarchical clustering, respectively.

626 ## Declarations

627 **Acknowledgments**

628 We thank Lausanne Genomic Technologies Facility and Vital-IT staff for high-throughput
629 sequencing and computational support. DG acknowledges support by: Swiss National Science
630 Foundation (grants 128399, 157528); National Centre of Competence in Research (NCCR) RNA
631 & Disease; Fondation Pierre Mercier; Fondation Leenaards; Olga Mayenfisch Stiftung;
632 SystemsX.ch StoNets consortium; University of Lausanne. PJ was supported by Human Frontiers
633 Science Program long-term fellowship LT000158/2013-L.

634 .

635 **Electronic supplementary material**

636 CasteloSzekely_Suppl.pdf: This file contains the Supplementary Figures S1-S14

637 CasteloSzekely_Suppl_Table_S1.xls: This file contains information on the deep-sequencing data
638 from kidney (raw read counts, mapping summary etc.)

639 CasteloSzekely_Suppl_Table_S2.xls: This file contains details of the GO-term analysis on the
640 differential TE gene set of Figure 2.

641 CasteloSzekely_Suppl_Table_S3.xls: This file contains the outcome of the transcriptome-wide
642 rhythmicity analyses on the kidney datasets (related to Figure 3A).

643 CasteloSzekely_Suppl_Table_S4.xls: This file contains the outcome of the rhythmicity analyses
644 in kidney and liver for the 178 commonly rhythmic genes (related to Figure 3C).

645 Supp_dataset_S1.zip: This zip-file contains transcriptome-wide, time-resolved expression plots
646 for kidney RPF (blue) and RNA (orange) in the left panels (with “error bars” connecting the
647 two replicates of each timepoint) and TE in the right panels.

648 Supp_dataset_S2.zip: Similar to Supp_dataset_S2.zip, expression plots for kidney and liver for
649 the 178 common rhythmic genes of Figure 3C.

650 **Competing interests**

651 The authors declare that they have no competing interests.

652 **Author contributions**

653 VCS and PJ performed the experiments. VCS and ABA analysed the data. DG and VCS wrote
654 the manuscript with inputs from the others authors. DG designed the project.

655 ## References

656 1. Dibner C, Schibler U, Albrecht U: **The mammalian circadian timing system:**
657 **organization and coordination of central and peripheral clocks.** *Annu Rev Physiol*
658 2010, **72:**517-549.

659 2. Partch CL, Green CB, Takahashi JS: **Molecular architecture of the mammalian**
660 **circadian clock.** *Trends Cell Biol* 2014, **24:**90-99.

661 3. Zhang R, Lahens NF, Ballance HI, Hughes ME, Hogenesch JB: **A circadian gene**
662 **expression atlas in mammals: Implications for biology and medicine.** *Proc Natl*
663 *Acad Sci U S A* 2014, **111:**16219-16224.

664 4. Meireles-Filho AC, Bardet AF, Yanez-Cuna JO, Stampfel G, Stark A: **cis-Regulatory**
665 **Requirements for Tissue-Specific Programs of the Circadian Clock.** *Curr Biol*
666 2014, **24:**1-10.

667 5. Yoo SH, Yamazaki S, Lowrey PL, Shimomura K, Ko CH, Buhr ED, Siepka SM, Hong HK,
668 Oh WJ, Yoo OJ, et al: **PERIOD2::LUCIFERASE real-time reporting of circadian**
669 **dynamics reveals persistent circadian oscillations in mouse peripheral tissues.**
670 *Proc Natl Acad Sci U S A* 2004, **101:**5339-5346.

671 6. Luck S, Westermark PO: **Circadian mRNA expression: insights from modeling and**
672 **transcriptomics.** *Cell Mol Life Sci* 2016, **73:**497-521.

673 7. Reddy AB, Karp NA, Maywood ES, Sage EA, Deery M, O'Neill JS, Wong GK, Chesham J,
674 Odell M, Lilley KS, et al: **Circadian orchestration of the hepatic proteome.** *Curr Biol*
675 2006, **16:**1107-1115.

676 8. Mauvoisin D, Wang J, Jouffe C, Martin E, Atger F, Waridel P, Quadroni M, Gachon F,
677 Naef F: **Circadian clock-dependent and -independent rhythmic proteomes**
678 **implement distinct diurnal functions in mouse liver.** *Proc Natl Acad Sci U S A*
679 2014, **111:**167-172.

680 9. Robles MS, Cox J, Mann M: **In-vivo quantitative proteomics reveals a key**
681 **contribution of post-transcriptional mechanisms to the circadian regulation of**
682 **liver metabolism.** *PLoS Genet* 2014, **10:**e1004047.
683 10. Janich P, Arpat AB, Castelo-Szekely V, Lopes M, Gatfield D: **Ribosome profiling**
684 **reveals the rhythmic liver translatome and circadian clock regulation by**
685 **upstream open reading frames.** *Genome Res* 2015, **25:**1848-1859.
686 11. Atger F, Gobet C, Marquis J, Martin E, Wang J, Weger B, Lefebvre G, Descombes P, Naef
687 F, Gachon F: **Circadian and feeding rhythms differentially affect rhythmic mRNA**
688 **transcription and translation in mouse liver.** *Proc Natl Acad Sci U S A* 2015,
689 **112:**E6579-6588.
690 12. Jouffe C, Cretenet G, Symul L, Martin E, Atger F, Naef F, Gachon F: **The circadian clock**
691 **coordinates ribosome biogenesis.** *PLoS Biol* 2013, **11:**e1001455.
692 13. Bonny O, Vinciguerra M, Gumz ML, Mazzoccoli G: **Molecular bases of circadian**
693 **rhythmicity in renal physiology and pathology.** *Nephrol Dial Transplant* 2013,
694 **28:**2421-2431.
695 14. Ingolia NT: **Ribosome profiling: new views of translation, from single codons to**
696 **genome scale.** *Nat Rev Genet* 2014, **15:**205-213.
697 15. Brawand D, Soumillon M, Necsulea A, Julien P, Csardi G, Harrigan P, Weier M, Liechti
698 A, Aximu-Petri A, Kircher M, et al: **The evolution of gene expression levels in**
699 **mammalian organs.** *Nature* 2011, **478:**343-348.
700 16. Janich P, Arpat AB, Castelo-Szekely V, Gatfield D: **Analyzing the temporal regulation**
701 **of translation efficiency in mouse liver.** *Genom Data* 2016, **8:**41-44.
702 17. O'Connor PB, Andreev DE, Baranov PV: **Comparative survey of the relative impact**
703 **of mRNA features on local ribosome profiling read density.** *Nat Commun* 2016,
704 **7:**12915.

705 18. Albert FW, Muzzey D, Weissman JS, Kruglyak L: **Genetic influences on translation in**
706 **yeast.** *PLoS Genet* 2014, **10:**e1004692.
707 19. Schafer S, Adami E, Heinig M, Rodrigues KE, Kreuchwig F, Silhavy J, van Heesch S,
708 Simaite D, Rajewsky N, Cuppen E, et al: **Translational regulation shapes the**
709 **molecular landscape of complex disease phenotypes.** *Nat Commun* 2015, **6:**7200.
710 20. Gonzalez-Porta M, Calvo M, Sammeth M, Guigo R: **Estimation of alternative splicing**
711 **variability in human populations.** *Genome Res* 2012, **22:**528-538.
712 21. Kojima S, Sher-Chen EL, Green CB: **Circadian control of mRNA polyadenylation**
713 **dynamics regulates rhythmic protein expression.** *Genes Dev* 2012, **26:**2724-2736.
714 22. Olshen AB, Hsieh AC, Stumpf CR, Olshen RA, Ruggero D, Taylor BS: **Assessing gene-**
715 **level translational control from ribosome profiling.** *Bioinformatics* 2013,
716 **29:**2995-3002.
717 23. Lee Y, Chen R, Lee HM, Lee C: **Stoichiometric relationship among clock proteins**
718 **determines robustness of circadian rhythms.** *J Biol Chem* 2011, **286:**7033-7042.
719 24. Yagita K, Horie K, Koinuma S, Nakamura W, Yamanaka I, Urasaki A, Shigeyoshi Y,
720 Kawakami K, Shimada S, Takeda J, Uchiyama Y: **Development of the circadian**
721 **oscillator during differentiation of mouse embryonic stem cells in vitro.** *Proc*
722 *Natl Acad Sci U S A* 2010, **107:**3846-3851.
723 25. Landgraf D, Wang LL, Diemer T, Welsh DK: **NPAS2 Compensates for Loss of CLOCK**
724 **in Peripheral Circadian Oscillators.** *PLoS Genet* 2016, **12:**e1005882.
725 26. Fang B, Lazar MA: **Dissecting the Rev-erbalpha Cistrome and the Mechanisms**
726 **Controlling Circadian Transcription in Liver.** *Cold Spring Harb Symp Quant Biol*
727 2015, **80:**233-238.
728 27. D'Alessandro M, Beesley S, Kim JK, Chen R, Abich E, Cheng W, Yi P, Takahashi JS, Lee
729 C: **A tunable artificial circadian clock in clock-defective mice.** *Nat Commun* 2015,
730 **6:**8587.

731 28. Gu X, Xing L, Shi G, Liu Z, Wang X, Qu Z, Wu X, Dong Z, Gao X, Liu G, et al: **The**
732 **circadian mutation PER2(S662G) is linked to cell cycle progression and**
733 **tumorigenesis.** *Cell Death Differ* 2012, **19:**397-405.
734 29. Ingolia NT, Ghaemmaghami S, Newman JR, Weissman JS: **Genome-wide analysis in**
735 **vivo of translation with nucleotide resolution using ribosome profiling.** *Science*
736 2009, **324:**218-223.
737 30. McManus CJ, May GE, Spealman P, Shteyman A: **Ribosome profiling reveals post-**
738 **transcriptional buffering of divergent gene expression in yeast.** *Genome Res*
739 2014, **24:**422-430.
740 31. Khan Z, Ford MJ, Cusanovich DA, Mitrano A, Pritchard JK, Gilad Y: **Primate transcript**
741 **and protein expression levels evolve under compensatory selection pressures.**
742 *Science* 2013, **342:**1100-1104.
743 32. Schrimpf SP, Weiss M, Reiter L, Ahrens CH, Jovanovic M, Malmstrom J, Brunner E,
744 Mohanty S, Lercher MJ, Hunziker PE, et al: **Comparative functional analysis of the**
745 **Caenorhabditis elegans and Drosophila melanogaster proteomes.** *PLoS Biol*
746 2009, **7:**e48.
747 33. Jang C, Lahens NF, Hogenesch JB, Sehgal A: **Ribosome profiling reveals an**
748 **important role for translational control in circadian gene expression.** *Genome*
749 *Res* 2015, **25:**1836-1847.
750 34. Dunlap JC: **Genetics and molecular analysis of circadian rhythms.** *Annu Rev Genet*
751 1996, **30:**579-601.
752 35. Martin M: **Cutadapt removes adapter sequences from high-throughput**
753 **sequencing reads.** *EMBnetjournal* 2011, **17:**10-12.
754 36. Langmead B, Salzberg SL: **Fast gapped-read alignment with Bowtie 2.** *Nat Methods*
755 2012, **9:**357-359.
756 37. Trapnell C, Pachter L, Salzberg SL: **TopHat: discovering splice junctions with RNA-**
757 **Seq.** *Bioinformatics* 2009, **25:**1105-1111.

758 38. Trapnell C, Williams BA, Pertea G, Mortazavi A, Kwan G, van Baren MJ, Salzberg SL,
759 Wold BJ, Pachter L: **Transcript assembly and quantification by RNA-Seq reveals**
760 **unannotated transcripts and isoform switching during cell differentiation.** *Nat*
761 *Biotechnol* 2010, **28:**511-515.
762 39. Robinson MD, Oshlack A: **A scaling normalization method for differential**
763 **expression analysis of RNA-seq data.** *Genome Biol* 2010, **11:**R25.
764 40. Warton DI, Wright IJ, Falster DS, Westoby M: **Bivariate line-fitting methods for**
765 **allometry.** *Biol Rev Camb Philos Soc* 2006, **81:**259-291.
766 41. Lorenz R, Bernhart SH, Honer Zu Siederdissen C, Tafer H, Flamm C, Stadler PF,
767 Hofacker IL: **ViennaRNA Package 2.0.** *Algorithms Mol Biol* 2011, **6:**26.
768

769 ## Figure legends

770 **Fig. 1. Ribosome profiling around-the-clock in mouse liver and kidney.**

771 **A** Overview of the experimental design. Livers and kidneys for ribosome profiling were collected
772 every 2 hours for two daily cycles. Each timepoint sample was a pool of organs from two animals.
773 Mice were kept under 12 hour:12 hour light-dark conditions, with *Zeitgeber* times ZT00
774 corresponding to lights-on and ZT12 to lights-off.

775 **B** Read distribution to transcript features. RPF-seq (left; kidney in orange, liver in green) and
776 RNA-seq (right; blue and red for kidney and liver, respectively) compared to a distribution
777 expected from the relative feature sizes (grey; the distributions based on feature sizes were highly
778 similar for both organs, thus only that for kidney is shown). Note that RPF-seq footprints were
779 enriched on the CDS and depleted from UTRs, whereas RNA-seq reads distributed more
780 homogeneously along transcripts, according to feature size. Of note, the higher level of 3′ UTR
781 footprints in kidney resulted mainly from differences in the efficiency with which stop codon
782 footprints were captured, as described in panel C.

783 **C** Predicted position of the ribosome's aminoacyl tRNA-site (A-site) of reads relative to the CDS
784 start and stop codons. Read density at each position was averaged across single protein coding
785 isoform genes (i.e., genes with one main expressed transcript isoform) that had an average RPF
786 RPKM >5, a CDS >400 nt in length and were expressed in both organs (N=3037 genes). This
787 analysis revealed the trinucleotide periodicity of RPF-seq (but not RNA-seq) reads in both organs.
788 Inset: Frame analysis of CDS reads showed preference for the annotated reading frame (frame 1,
789 the same frame as the start codon) in RPF but not in RNA reads. Violin plots extend to the range
790 of the data (N=3694 genes for liver, N=4602 genes for kidney). A separate analysis of the higher
791 level of stop codon footprints in kidney, that also led to the differences in 3′ UTR reads in B, can
792 be found in Figure S2A-B.

793 **D** Principal component (PC) analysis of kidney and liver RPF-seq and RNA-seq datasets, using
794 the 4000 most variable genes. The first two components reflected the variability coming from
795 organ (PC1, 64.21%) and from RPF/RNA origin of datasets (PC2, 28.35%).

796 **E** PC3 vs. PC5 (together 12.5% of variation) resolved the factor time within each dataset, leading
797 to a representation that resembled the face of a clock. Each dot represents one sample, timepoint

798 replicates are joined by a line and timepoints within each dataset are sequentially coloured. The
799 circular arrangement was larger for liver than kidney, suggesting a higher contribution of hepatic
800 rhythmic genes to overall variability. Figure S4 shows the scree plot for the ten first components.

801 **Fig. 2. Cross-organ differences in translation efficiency partially compensate RNA**
802 **abundance differences and show association with transcript features.**
803 **A** Venn diagram showing the gene expression overlap (i.e. genes detected at both RPF and RNA
804 level) between kidney (yellow, N=12423 genes) and liver (green, N=10676 genes). Same cut-offs
805 on RPKM (reads per kilobase of transcript per million mapped reads) were used for both organs.
806 **B** Scatterplot of kidney-to-liver ratio of mRNA abundance vs. translation efficiency (TE) for all
807 expressed genes (N=10289), averaged over all timepoints. Corresponding density curves are
808 plotted on the margins. Dashed red lines represent the 2.5 and 97.5 percentiles of each variable,
809 and the corresponding fold-change is indicated. Linear regression line is depicted in blue
810 (R^2=0.0009, p=0.0009). While 95% of genes spanned a 114-fold range in mRNA abundance
811 differences across organs, the same number of genes changed less than 3-fold in TE, underlining
812 that transcript abundance was the main contributor to divergent gene expression.
813 **C** Inter-organ Spearman correlation for RNA-seq and RPF-seq samples. Each dot represents the
814 correlation coefficient between kidney and liver for a timepoint and replicate sample. Note that
815 RPF-seq samples consistently correlated significantly better than RNA-seq samples did (p<2.2e-
816 16, N=24, paired t-test of Fisher-transformed correlation coefficients).
817 **D** Scatterplot of inter-organ RNA vs. RPF correlation coefficients for each sample separately
818 calculated from all (blue, N=10289), from single isoform (red, N=5815), and from multiple isoform
819 (pink, N=4474) genes. Consistently better RPF correlation was evident in all cases.
820 **E** Relative TE in liver vs. kidney (data centred and averaged over all timepoints for all expressed
821 genes, N=10289) showed an overall strong inter-organ correlation. Differential TE – defined as
822 having FDR-corrected p<0.01 (Wilcoxon signed rank test on TE) and >1.5 difference in TE across
823 organs – was apparent for ca. 9% of genes (yellow and green show cases where TE is higher in
824 kidney and liver, respectively, N=960).
825 **F** Cumulative distribution of Hellinger distances for genes showing differential TE (red, N=960), or

826 not (grey, N=9329), as detected in (E). Hellinger distance was used as a quantitative measure for
827 relative transcript isoform diversity across organs, as described in Results and Methods. The
828 analysis shows that divergent TE correlated with larger diversity in transcript isoform expression
829 (D=0.0702, p=3.74e-04, two-sample Kolmogorov-Smirnov [KS] test).
830 **G** Cumulative distribution of the kidney-to-liver TE ratio for genes whose transcript diversity
831 originated exclusively from the 5′ UTR (identical CDS and 3' UTR, light blue, N=216; these genes
832 show more TE differences across organs), and genes whose transcripts had identical 5′ UTR
833 (and divergent CDS and/or 3′ UTR, purple, N=314; these genes show less TE differences across
834 organs). The vertical dashed grey line marks the 1.5-fold difference used to define differential TE
835 (as in (E)). These results suggested that tissue specificity in TE was partially achieved by
836 expressing transcript isoforms that differed in their 5′ UTRs (note the significant shift towards
837 smaller TE differences for genes with identical 5' UTRs). See also Figure S9.

838 **Fig. 3. Rhythmicity analyses across organs reveals phase modulation by translation in**
839 **kidney.**
840 **A** Venn diagram showing rhythmic genes in kidney. Of the 12423 expressed genes, 1338 showed
841 24-hour oscillations of >1.5-fold amplitude in mRNA abundance (RNA-seq, 10.7%) and 977 in
842 footprint abundance (RPF-seq, 7.9%). 542 genes (4.3%) were identified as rhythmic at both
843 levels.
844 **B** Cumulative distribution of phase differences (RPF peak – RNA peak, in hours) for genes
845 rhythmic at both RNA-seq and RPF-seq in liver (green, N=1178) and kidney (yellow, N=542). The
846 two distributions were significantly different (p<1e-04, permutation test), and reflected that
847 maximal footprint abundance frequently preceded mRNA abundance peaks in kidney (note that
848 the two distributions differed mostly in their negative tail).
849 **C** 4-way Venn diagram of rhythmicity sets for genes expressed in both tissues (N=10289). 364
850 and 238 genes were detected as rhythmic in both organs at the RNA-seq and RPF-seq levels,
851 respectively, and 178 genes were detected as rhythmic throughout (i.e. RNA-seq and RPF-seq, in
852 kidney and liver).
853 **D** Cumulative phase difference distribution in liver (green) and kidney (yellow) for the 178

854 common rhythmic genes. As in (B), the distributions were significantly different (p=0.007,
855 permutation test), and corroborated that even when comparing the same set of genes, footprint
856 peaks frequently preceded mRNA abundance maxima in kidney.
857 **E** Cross-correlation in kidney (yellow) and liver (green) of time-resolved RPF-seq profiles relative
858 to the RNA-seq profiles of the N=178 common rhythmic genes. The analysis showed that profile
859 correlations for negative lags (i.e. RPF peaking before RNA) were significantly higher in kidney
860 than liver (asterisks indicate $p<0.05$, Wilcoxon signed rank test). Boxplots represent the
861 interquartile range and whiskers extend to the minimum and maximum expression within 1.5
862 times the interquartile range.
863 **F** Examples for genes with maxima in RPF (blue) preceding those in RNA (orange) by several
864 hours in kidney (top) but not, or less so, in liver (bottom). Arrowheads indicate the peaks in
865 footprint and mRNA abundance as estimated from the rhythmic fits.
866 **G** Cross-correlation analyses of RPF-seq relative to RNA-seq profiles (kidney in yellow, liver in
867 green) for the genes in (F). Maximal correlations of the profiles in kidney were found to be shifted
868 to the left (more negative RPF-to-RNA lags) as compared to liver. For liver, there was no case
869 with a maximal correlation value in the negative.

870 **Fig. 4. High tissue divergence in translationally driven rhythms.**
871 **A** Venn diagram of rhythmic RPF-seq sets in kidney (yellow, N=92) and liver (green, N=142) after
872 the Babel analysis indicated strong tissue-specificity of translational control.
873 **B** Daily profiles of RPF-seq RPKM (blue) and RNA-seq RPKM (orange) for the two genes
874 detected as translationally regulated in both tissues in A.
875 **C** and **D** Circular phase histogram for the 92 (C, kidney) and 142 (D, liver) genes showing
876 footprint rhythmicity in the organs. Note that the translational upregulation of transcripts observed
877 at the day-to-night transition in liver was absent in kidney.
878 **E** and **F** Heatmaps of RNA (left panels) and RPF (right panels) rhythms for the 92 and 142 genes
879 translationally regulated in kidney (E) and in liver (F), respectively. Genes are sorted by footprint
880 phase and expression levels are standardized by row (gene). These sets of genes showed
881 rhythmicity in footprint abundance but no oscillation in mRNA.

882 **G** and **H** Daily profiles of RPF-seq RPKM (blue) and RNA-seq RPKM (orange) for representative
883 examples of translationally generated rhythms specific for liver (G) and kidney (H). For each
884 gene, the upper panel shows the kidney data and the lower panel the liver data. *Hoxd3* was not
885 expressed in liver.
886 **I** Translation efficiency (TE) around-the-clock for ribosomal protein (RP) genes expressed in liver
887 (green, N=86) and in kidney (yellow, N=89). For each timepoint (ZT) boxplots represent the
888 interquartile range and whiskers extend to the minimum and maximum TE within 1.5 times the
889 interquantile range. Lines connect the median of each boxplot to ease visualization. Note the
890 global TE upregulation at ZT10 in liver, whereas TEs in kidney remain high over the day.

891 **Figure 5. Tissue specificity in core clock gene expression at the level of RNA abundance**
892 **and translation.**
893 **A** Scatterplot of transcript abundance (RNA-seq) vs. footprint abundance (RPF-seq) for liver
894 (grey) and kidney (sepia) (N=10289), where core clock components are highlighted (kidney dots
895 with dashed circles). Coloured dashed lines join the relative locations of each core clock gene
896 between organs.
897 **B** Bar graph of the average RPKM ratio between kidney and liver for the main circadian core
898 clock genes, at the level of mRNA abundance (dark shades) and ribosome footprints (light
899 shades) suggested that translational compensation led to higher similarity at the level of protein
900 biosynthesis (RPF) for several core clock genes.
901 **C** Hierarchical clustering of the organs' RNA and RPF profiles based on the similarities of the
902 core clock genes expression patterns (N=12, genes shown in B). The height of the branches
903 represents weighted average distances over the considered genes (see Methods). Note that RPF
904 rhythms in two organs were more similar than RNA and RPF rhythms within an organ.
905 **D** Hierarchical clustering as in C based on the genes detected as rhythmic throughout (N=178,
906 see Figure 3C). When compared to the clustering based on core clock gene expression patterns
907 in C, this rhythmic gene set showed an organ-based clustering.
908 **E** Scatterplot of kidney/liver ratios of uORF vs. CDS translation efficiencies for genes containing
909 AUG-initiated translated uORFs in both organs (N=1199). uORF-containing core clock genes are

910 highlighted. As also shown in Fig S8E, differential uORF usage could not globally explain
911 differences in CDS TE across organs (note the lack of negative correlation between the two
912 variables, R^2 = 0.005, p=0.008). As an exception, the lower uORF TE of *Nr1d2* might have a role
913 in setting relatively higher CDS TE in kidney.

914 **F** RPF (blue) and RNA (orange) reads mapping along the *Nr1d2* transcript in kidney (top) and
915 liver (bottom) for the timepoint of maximal CDS translation (ZT10). 5′ UTR and CDS are shown in
916 full, but for better visualization only a portion of the 3′ UTR (the same length as the 5′ UTR) is
917 shown. Red boxes indicate the predicted AUG-initiated translated uORFs. Right panels show
918 that, similar to the CDS, the uORFs showed clear frame preference, indicative of active
919 translation.

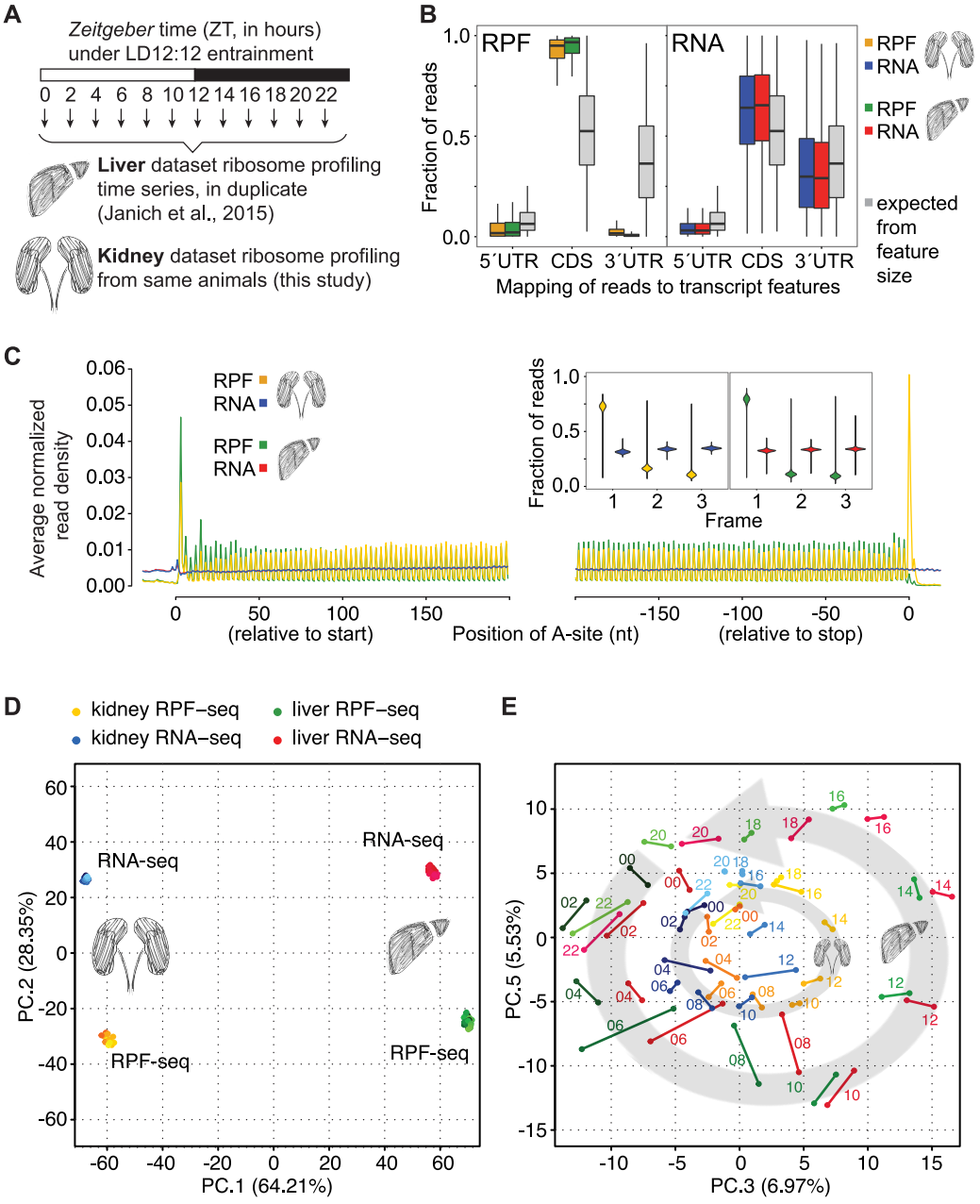
A
Zeitgeber time (ZT, in hours)
under LD12:12 entrainment
0 2 4 6 8 10 12 14 16 18 20 22
Liver dataset ribosome profiling
time series, in duplicate
(Janich et al., 2015)
Kidney dataset ribosome profiling
from same animals (this study)
B
RPF
RNA
Fraction of reads
1.0
0.5
0.0
5´UTR CDS 3´UTR 5´UTR CDS 3´UTR
Mapping of reads to transcript features
RPF
RNA
RPF
RNA
expected
from
feature
size
C
Average normalized
read density
0.06
0.05
0.04
0.03
0.02
0.01
0.00
RPF
RNA
RPF
RNA
0 50 100 150
(relative to start)
Position of A-site (nt)
Fraction of reads
1.0
0.5
0.0
1 2 3 1 2 3
Frame
-150 -100 -50 0
(relative to stop)
D
kidney RPF–seq
kidney RNA–seq
liver RPF–seq
liver RNA–seq
RNA-seq
RNA-seq
RPF-seq
RPF-seq
PC.2 (28.35%)
PC.1 (64.21%)
E
PC.5 (5.53%)
PC.3 (6.97%)

Castelo-Szekely_Fig2

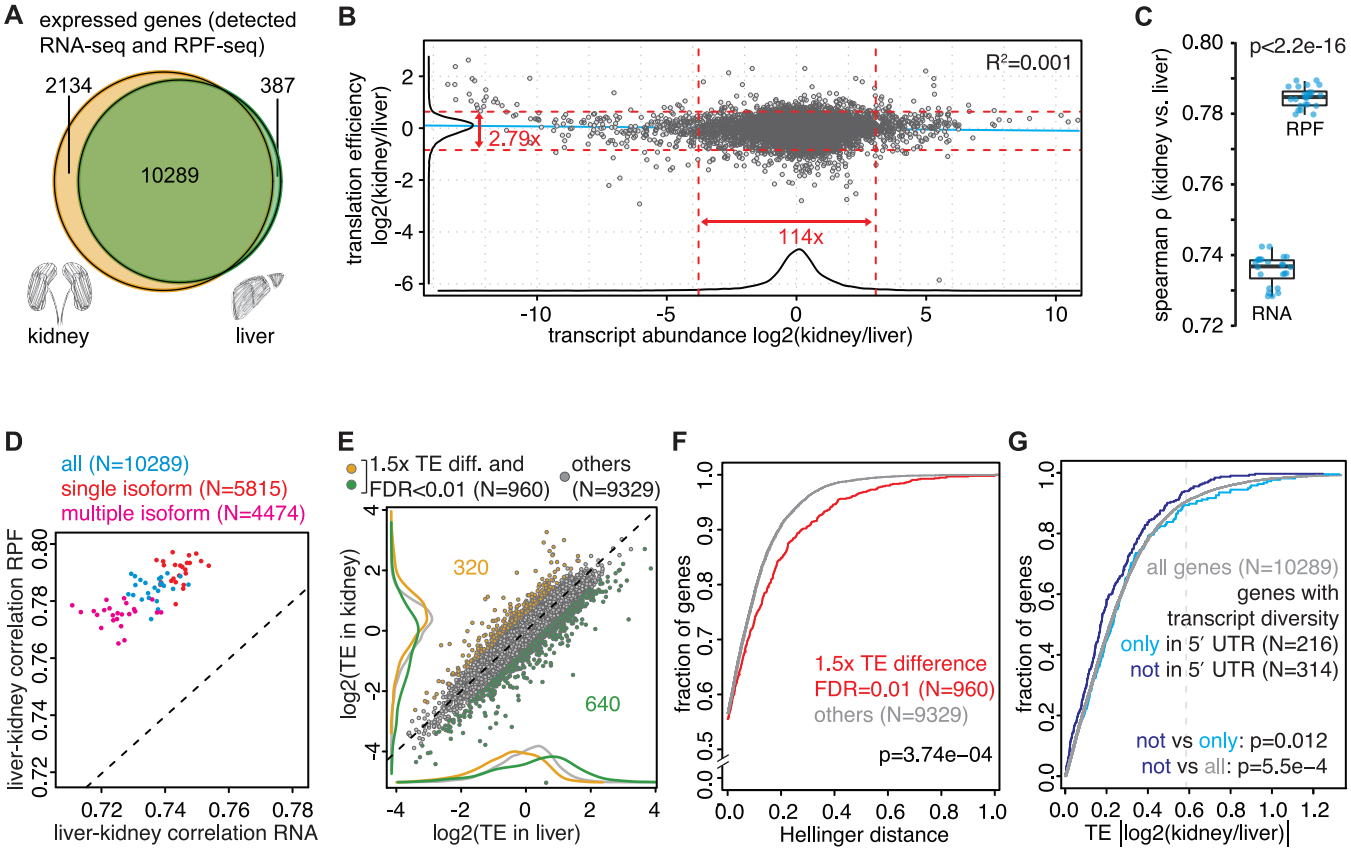

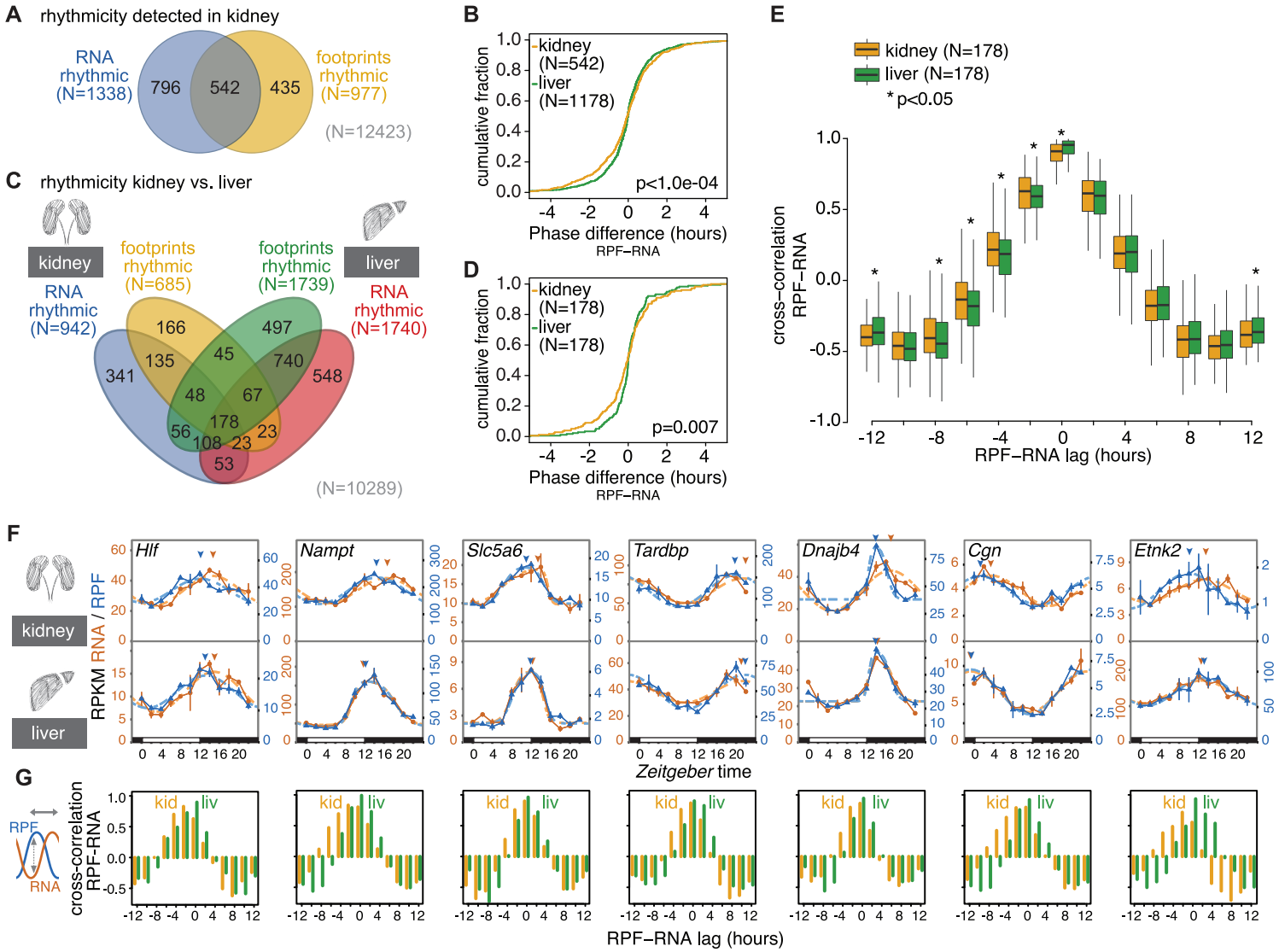
A
rhythmicity detected in kidney
RNA rhythmic (N=1338)
796
542
435
footprints rhythmic (N=977)
(N=12423)
B
kidney (N=542)
liver (N=1178)
cumulative fraction
p<1.0e-04
Phase difference (hours)
RPF−RNA
C
rhythmicity kidney vs. liver
kidney
liver
RNA rhythmic (N=942)
footprints rhythmic (N=685)
footprints rhythmic (N=1739)
RNA rhythmic (N=1740)
166
497
135
45
740
341
548
48
67
178
56
108
23
23
53
(N=10289)
D
kidney (N=178)
liver (N=178)
cumulative fraction
p=0.007
Phase difference (hours)
RPF−RNA
E
kidney (N=178)
liver (N=178)
* p<0.05
cross−correlation RPF−RNA
RPF−RNA lag (hours)
F
kidney
liver
RPKM RNA / RPF
Hlf
Nampt
Slc5a6
Tardbp
Dnajb4
Cgn
Etnk2
Zeitgeber time
G
RPF
RNA
cross-correlation RPF-RNA
kid
liv
RPF−RNA lag (hours)

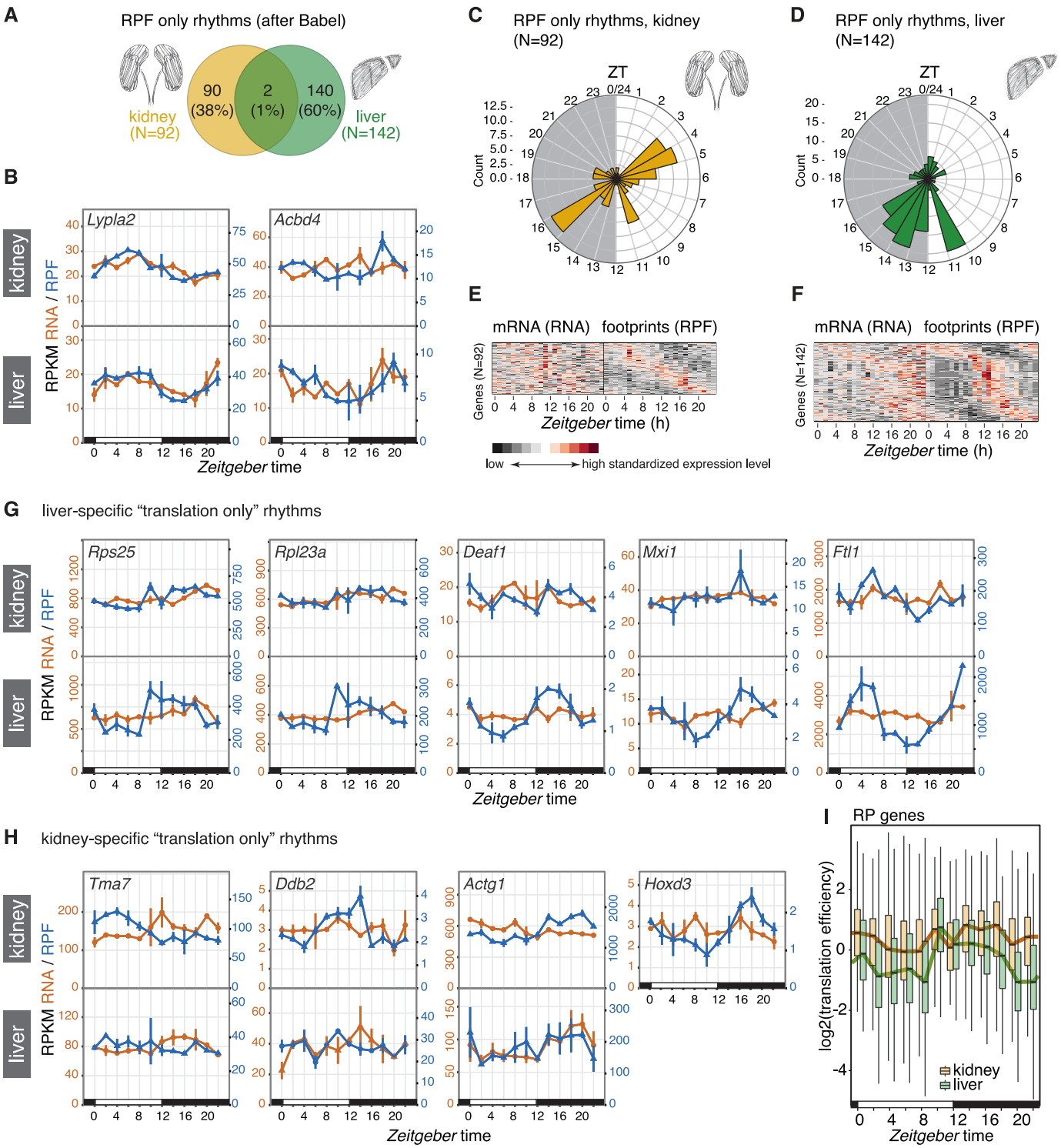
A
RPF only rhythms (after Babel)
kidney (N=92)
90 (38%)
2 (1%)
140 (60%)
liver (N=142)
B
kidney
liver
RPKM RNA / RPF
Lypla2
Acbd4
Zeitgeber time
C
RPF only rhythms, kidney (N=92)
ZT
Count
D
RPF only rhythms, liver (N=142)
E
mRNA (RNA)
footprints (RPF)
Genes (N=92)
Zeitgeber time (h)
low
high standardized expression level
F
Genes (N=142)
G
liver-specific "translation only" rhythms
Rps25
Rpl23a
Deaf1
Mxi1
Ftl1
H
kidney-specific "translation only" rhythms
Tma7
Ddb2
Actg1
Hoxd3
I
RP genes
log2(translation efficiency)
kidney
liver

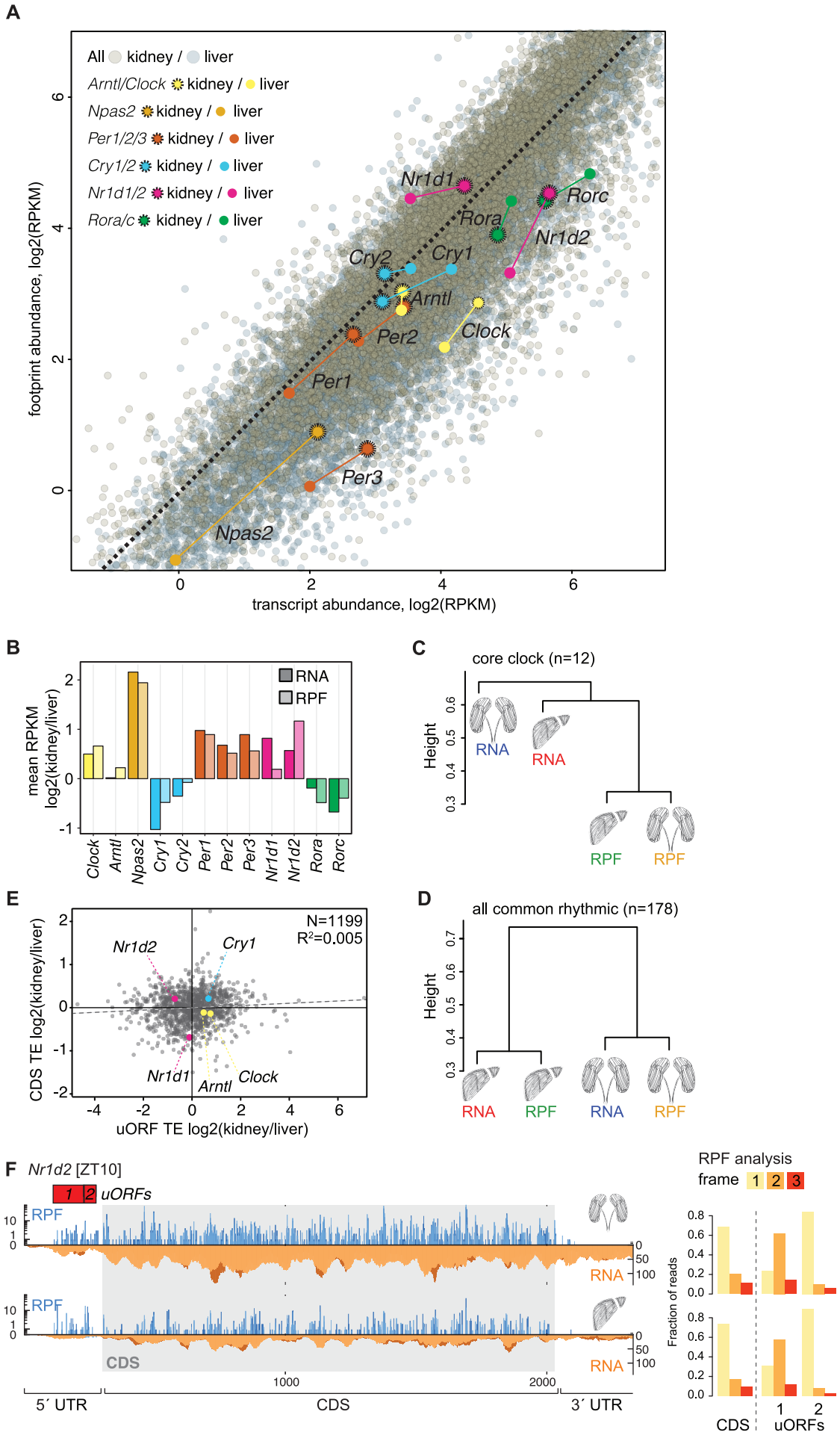
A
All kidney / liver
Arntl/Clock kidney / liver
Npas2 kidney / liver
Per1/2/3 kidney / liver
Cry1/2 kidney / liver
Nr1d1/2 kidney / liver
Rora/c kidney / liver
footprint abundance, log2(RPKM)
transcript abundance, log2(RPKM)
Nr1d1
Rorc
Rora
Nr1d2
Cry2
Cry1
Arntl
Clock
Per2
Per1
Per3
Npas2
B
mean RPKM log2(kidney/liver)
RNA
RPF
Clock
Arntl
Npas2
Cry1
Cry2
Per1
Per2
Per3
Nr1d1
Nr1d2
Rora
Rorc
C
core clock (n=12)
Height
RNA
RNA
RPF
RPF
E
N=1199
R²=0.005
CDS TE log2(kidney/liver)
uORF TE log2(kidney/liver)
Nr1d2
Cry1
Nr1d1
Arntl
Clock
D
all common rhythmic (n=178)
Height
RNA
RPF
RNA
RPF
F
Nr1d2 [ZT10]
1 2 uORFs
RPF
RNA
CDS
5′ UTR
CDS
3′ UTR
RPF analysis
frame 1 2 3
Fraction of reads
CDS
uORFs

SUPPLEMENTARY FIGURE LEGENDS

Translational contributions to tissue-specificity in rhythmic and constitutive gene expression

Violeta Castelo-Szekely, Alaaddin Bulak Arpat, Peggy Janich, David Gatfield

Figure S1. Overview of sequencing outcome and read length distribution for RPF- and RNA-seq data used in the study.

A Summary of outcome of the sequential mapping pipeline, indicating the number (y-axis) and percentage (within bars) of reads mapping to each database, averaged over all timepoints. For each sample of the four datasets an average of more than 20 million reads mapped to the protein-coding transcriptome (cDNA) and was used for the study.

B and C RPF-seq (B) and RNA-seq (C) read length after trimming of adaptors showed that most RPF-seq reads had a length of 29-30 nucleotides in both organs, whereas RNA-seq fragments showed a broader distribution as expected from chemical RNA fragmentation. Boxplots represent the interquartile range and whiskers extend to the minimum and maximum values within 1.5 times the interquartile range.

Figure S2. RPF reads at the stop codon and quality control.

A A-site position of RPF-seq reads in the last 200 nt of the CDS, excluding stop codon reads. Read density along the CDS was similar in liver and kidney; thus the higher read density observed in Fig. 1C at the stop codon does not affect CDS-based calculations.

B Zooming into the footprint read density at the end of the CDS, stop codon, and beginning of the 3′ UTR indicated read differences between organs for the stop codon itself and up to 4 nt downstream, which were increased in kidney. Stop codon reads are counted towards the 3′ UTR and their higher level in kidney thus also explains why our analysis in Fig. 1B shows more 3′ UTR reads for this organ. The remainder of the 3′ UTR shows a similar depletion of reads in both organs.

C and D Ribo-seq Unit Step Transformation (RUST) metafootprint analyses to evaluate the contribution of local mRNA positions to the density of footprints. Light

and dark coloured polygonal areas denote the 10%-90% and 25%-75% percentiles, respectively, and the dash-line denotes the median of the Kullback–Leibler divergence (K–L) profiles of all samples within kidney (C) and liver (D) separately for RPF and RNA reads (colour code in inset). The K-L profile for each sample was calculated from the RUST ratio values of 61 sense codons across a moving window of 40 triplet codons upstream to 20 triplet codons downstream of predicted A-sites. High K-L divergence maxima (lowest relative entropy or highest information gain) are thus found in the vicinity of the A-site in RPF libraries, and the 5′ and 3′ termini of the reads in RNA libraries. Importantly, the profiles are similar for kidney and liver, indicating overall similar footprint quality in the two independent datasets.

Figure S3. High technical and biological reproducibility of datasets.

A and B Spearman correlation of normalised CDS read counts between timepoints and between replicates for kidney RPF-seq (A) and kidney RNA-seq (B) datasets. The correlation coefficient is indicated by the size and shading of the disks. Biological replicates thus show excellent correlation; moreover, the correlation coefficients of different timepoints reflect the rhythmic nature of the data.

C and D Normalised CDS read counts (RPKM) in liver vs. kidney at the RNA (C) and RPF level (D). In these graphs, the averages over all timepoints were compared for the set of commonly expressed genes (N=10289; see Fig. 2A). Note the overall higher Spearman correlation at the footprint level than transcript level. The difference between correlations is highly significant with p=8.7e-110, Z value=-22.23; Steiger test for difference between 2 dependent correlations (Reference: Steiger JH, 1980. Psychological Bulletin, 87, 245-251).

Figure S4. Additional information for Principal Component Analysis.

Scree plot showing the first 10 components of the PCA in Fig. 1D-E. Components 1 and 2 explained most variance, followed by PC3 to PC5, which explained a closely similar proportion of variance in the data; the plateau was apparent from the sixth

component.

Figure S5. Contribution of translation efficiency to overall gene expression variation within organs.

A and B Scatterplot of mRNA abundance vs. translation efficiency (TE) in kidney (A; N=12423 genes) and liver (B; N=10676 genes), averaged over all timepoints. Corresponding density lines are plotted on the margins. Dotted red lines represent the 2.5 and 97.5 percentiles, and the corresponding fold change is indicated. The transcript abundance range for 95% of genes thus spanned two orders of magnitude (>500-fold range in either organ), whereas TE dynamic range was less than 12-fold in either organ. Transcript abundance differences can thus be considered the main source of gene expression variability in the tissues. Moreover, Pearson's r values of 0.145 (kidney) and 0.196 (liver) indicate weak positive correlation of transcript abundance and TE.

C Scatterplot of transcript abundance (TA) vs. translation efficiency (TE) in main CDS for kidney and as averages over all timepoints. Highlighted are single protein-coding genes that contain (red) or do not contain (blue) translated uORFs. Corresponding density lines are plotted on the margins. uORF translation is thus clearly associated with significantly reduced translation efficiency. Numbers on the density curves indicate the location shift relative to all transcripts. Genes with translated uORFs: TA, p=0.16; TE, p<2.2e-16 (Wilcoxon rank sum test). Genes without translated uORFs: TA, p=8.7e-5; TE, p<2.2e-16 (Wilcoxon rank sum test).

Figure S6. Translational compensation is independent of technical biases in the datasets.

A and B Measurement error (ME) of all genes in the dataset (n=10289) was calculated separately for RNA-seq (red) and RPF-seq (turquoise) for kidney (A) and liver (B), and plotted as a function of increasing average expression levels. Briefly, measurement errors within each bin were calculated as in Albert et al., 2015 (Albert

FW, Muzzey D, Weissman JS, Kruglyak L, 2014. PLoS Genetics, 10, e1004692) using the 12 timepoints as replicates for the measurement estimates (see Methods).

C to E Spearman correlation between liver and kidney for RNA and RPF data for (C) genes showing the highest measurement errors (bin 1 in A, B), (D) bins 2-10, and (E) genes that have higher measurement error in RPF-seq than in RNA-seq samples in both organs (bins 7-10). Each boxplot contains the correlation coefficients between organs for each timepoint and replicate sample. Together these analyses showed that RPF-seq samples have a higher degree of similarity across organs (indicated p-values are from paired t-tests on Fisher-transformed correlation coefficients), even when considering lowly expressed genes with higher associated experimental error (C), or when considering genes with higher RPF-seq than RNA-seq measurement errors (E). These results thus ruled out that a systematic lower measurement error in RPF-seq experiments could have been the underlying cause of the higher correlation in RPF-seq than RNA-seq observed in Fig. 2C.

F and G Same as A and B, but with a filtered gene set in which specifically those genes that showed very different expression levels/high variability between organs or between datasets (RPF-seq, RNA-seq) were removed (see Methods). The reason to also analyse such a filtered set was that we wished to be sure that genes that were widely different in their gene expression level were not distorting the analyses (e.g. specifically causing extreme measurement errors under a condition where expression was very low). Moreover, because the binning into the groups was based on expression level across all sets (calculated as the fourth root of the product of liver RNA-seq, liver RPF-seq, kidney RNA-seq and kidney RPF-seq), the highly variable genes made binning inaccurate. This filtered set thus contained genes with overall better comparability across datasets; of note, the distribution of ME differences using the filtered set was very similar to the full set in A-B.

H to L Inter-organ Spearman correlation in RNA-seq and RPF-seq samples for various gene bins as indicated, using the filtered set. As in C-E, even when

114 considering for example the genes with the highest overall measurement error (H), or
115 the genes with higher RPF-seq than RNA-seq measurement errors in both organs
116 (L), a significantly higher correlation is observed in RPF-seq samples (paired t-test
117 on Fisher-transformed correlation coefficients).

118 **Figure S7. Translational compensation detected in rat liver and heart.**
119 **A)** Spearman correlation coefficient between rat heart and liver samples calculated
120 from the data of Schafer et al., 2015 (Schafer S, Adami E, Heinig M, Rodrigues KE,
121 Kreuchwig F, Silhavy J, van Heesch S, Simaite D, Rajewsky N, Cuppen E, Pravenec
122 M, Vingron M, Cook SA, Hubner N, 2015. Nature Communications 8, 7200). Each
123 boxplot contains the correlation coefficients of all possible pairwise comparisons
124 between heart and liver replicates (remark: in this study, organs in each of the five
125 replicates did not necessarily come from the same animals, thus precluding defined
126 pairwise comparisons between same animals). The indicated p-value is the 95th
127 percentile of the ensemble of p-values resulting from all possible comparisons
128 between RPF-seq and RNA-seq correlation coefficients (paired t-test of Fisher-
129 transformed coefficients). This analysis extended our observation of a globally higher
130 conservation between organs at the level of translational output (protein production)
131 than at the level of transcript abundance.
132 **B and C** Normalised CDS read counts (RPKM) in rat liver vs. heart at the RPF-seq
133 (B) and RNA-seq level (C), averaged over the five replicates used in the study of
134 Schafer et al., 2015. Note the overall higher Spearman correlation at the footprint
135 level as compared to the mRNA level. The difference between correlations is highly
136 significant with p=2.3e-201, Z value=-30.25; Steiger test for difference between 2
137 dependent correlations (Reference: Steiger JH, 1980. Psychological Bulletin, 87,
138 245-251).

139 **Figure S8. Analysis of transcript features with predictive value for differential**
140 **TE.**

A Cumulative distribution of the indicated transcript features for single isoform genes that do not show differential TE (black, n= 5278), or that show differential TE and either higher TE in kidney (yellow, N=193) or in liver (green, N=340). The indicated p-values are Kolmogorov-Smirnov test results of each group vs. 'all'. Statistically significant comparisons marked in red.

B Same as (A), but in the form of boxplots and using Wilcoxon rank-sum test for the differences between group means (again, marked in red, significant results).

C Fraction of single isoform genes with (blue) or without (red) translated uORFs in either organ. The group with differential and higher TE in liver contained significantly more translated uORF-containing transcripts than the genes not showing differential TE in either organ (p=6.08e-04; Fisher's exact test); for kidney, there was a slight depletion of uORF-containing transcripts (non-significant). This analysis indicates that uORF usage may play a role in setting TE differences across tissues. Note that in this analysis, we did not yet distinguish whether the uORF was translated in liver and/or kidney, but we treated the 1377 genes with a translated uORF in at least one organ as a single group.

D Organ-specific uORF usage and its association with differential TE. The group of genes with uORFs specifically translated in liver was enriched for transcripts better translated in in kidney, and vice versa, consistent with a role of tissue-specific uORF usage in setting TE differences. However, due to the low number of differential TE genes exhibiting uORF translation that was exclusive to one organ for this analysis, the enrichments and depletions did not reach statistical significance.

E Scatterplot of upstream ORF vs. CDS TE differences across organs for genes containing translated uORFs in both organs and detected as differential TE with higher TE in kidney (yellow) or liver (green), or not showing differential TE (grey). An anticorrelation between uORF usage and CDS TE was only observed for genes with differential and higher TE in liver.

168 **Figure S9. Relationship between transcript diversity and differential TE.**

169 **A** Cumulative distribution of the absolute kidney-to-liver TE ratio for genes whose
170 transcript diversity is present or absent only in the indicated feature. The vertical
171 dotted grey line marks the 1.5-fold difference used to define differential TE. In this
172 Figure, all 7 groups are plotted (transcript diversity only/not in 5′ UTR, CDS, 3′ UTR;
173 all genes); for better visibility, the analyses of individual features are also shown in
174 separate panels, i.e. in Fig. 2G (5′ UTR), Fig. S9B (CDS) and Fig. S9C (3′ UTR).
175 Collectively, these results showed that transcript diversity that originated only within
176 the CDS (red), or that was excluded from the 5′ UTR (purple), or that was present
177 only within the 3′ UTR (dark green), all showed smaller TE differences across
178 organs, thus pointing towards variability within the 5′ UTR as a contributor to tissue-
179 specific TE.

180 **B** As in (A) showing the genes with transcript diversity present (red) or absent
181 (orange) only in the CDS. Note that when transcript diversity is only in CDS (i.e.
182 UTRs are identical), there is a significant shift to more similar TEs in both organs.
183 This is consistent with the specific association of 5′ UTR diversity with differential TE
184 that is shown in Fig. 2G.

185 **C** As in (A) showing genes with transcript diversity present (dark green) or absent
186 (light green) only in the 3′ UTR.

187 **Figure S10. Analysis of phase differences in RNA and RPF rhythms in kidney**
188 **and across organs.**

189 **A** Histogram of phase differences (RPF – RNA, in hours) for all genes that were
190 detected as rhythmic in the kidney RPF and RNA data (N=542; see Fig. 3A).
191 Although the distribution mean was not significantly different from 0, more genes had
192 their footprint abundance peak advanced (N=282) than delayed (N=260) with respect
193 to their mRNA abundance peak.

194 **B and C** Histogram of the phase differences (footprints to mRNA abundance, in

195 hours) in kidney (B) and liver (C) for the 178 genes rhythmic in both organs (gene set
196 shown in Fig. 3C). We observed a broader distribution of phase differences in kidney
197 and globally a phase advance of RPF with respect to RNA (-0.143 hours), as
198 compared to overall stronger phase coherence of RPF and RNA in liver. See also
199 Figures 3D-E.
200 **D** Histogram of the differential (kidney – liver) phase difference (RPF – RNA) for the
201 178 genes that were rhythmic throughout (Fig. 3C). Although statistically not
202 reaching significance, the mean of -0.178 hours and the overall more genes for
203 which the phase difference had negative values (96 vs. 82 genes) were consistent
204 with the finding that RPF rhythms peak earlier than RNA rhythms specifically in
205 kidney.

206 **Figure S11. Higher expression of deadenylase complex subunits in kidney.**
207 **A and B** Daily expression profiles of the CCR4-NOT complex components in kidney
208 (A) and liver (B) at the RNA (orange) and RPF (blue) level.
209 **C** RPF expression of the CCR4-NOT subunits (averages over the day). Boxplots
210 represent the interquartile range and whiskers extend to the minimum and maximum
211 expression within 1.5 times the interquartile range. Note that differences in protein
212 biosynthesis are statistically significant for all subunits ($p<0.05$, two-sample t-test)
213 apart from *Cnot8*.

214 **Figure S12. Heatmaps of all detected RPF and RNA rhythms indicate false-**
215 **negatives of the rhythmicity detection method.**
216 **A** Same as Fig. 3A, but re-plotted here for ease of comparison with (B-D).
217 **B-D** Heatmap of RNA-seq (left) and RPF-seq (right) expression for genes detected
218 as rhythmic only at the mRNA level (B, N=796), at both levels (C, N=542), and at the
219 ribosome footprints only (D, N=435) in kidney. Gene expression levels are
220 standardised by row (gene). Please note that even the panels that should represent
221 “non-rhythmicity” (i.e. right panel in B and left panel in D) clearly showed underlying

222 rhythmicity, albeit with more noise and/or lower amplitude. Many of these cases were
223 therefore probably not truly “non-rhythmic” but rather false-negatives of the detection
224 method (see Results section).

225 **Figure S13. Core clock gene expression at RNA and RPF levels in both organs.**
226 **Left panels:** Daily expression profiles of the 12 main core clock genes shown in Fig.
227 5A-C. **Right panels:** Hierarchical clustering of the organs’ RNA and RPF profiles for
228 each clock gene. Branch height represent the average Euclidean distance. Note that
229 for 7 out of the 12 core clock genes, protein synthesis profiles were more conserved
230 across organs than mRNA abundance and than RPF-RNA within organs.

231 **Figure S14. Read distribution for uORF-containing core clock genes.**
232 **A** Normalised read distribution for RPF (in blue) and RNA (in orange) along core
233 clock transcripts containing uORFs in kidney (top) and liver (bottom) for the timepoint
234 of maximal CDS translation. Red boxes indicate AUG-initiated uORFs as predicted in
235 our analyses. For scaling issues and better visualisation, only a portion of the 3′
236 UTRs, corresponding to the same length as the full 5′ UTR, is depicted (exception
237 *Nr1d1*, for which the 3′ UTR is so short that it is shown full length).
238 **B** Read distribution to the three translation frames showed a frame bias of footprint
239 reads for most predicted uORFs that was in a similar range as the frame bias on the
240 CDS. This frame preference is indicative of active translation on the uORFs.

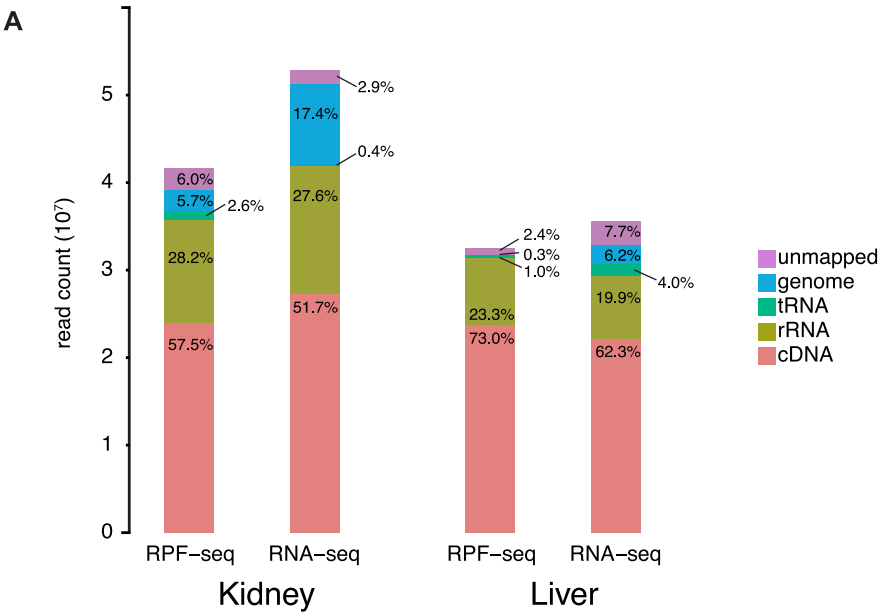
A
read count (10^7)
0
1
2
3
4
5
6.0%
5.7%
2.6%
28.2%
57.5%
2.9%
17.4%
0.4%
27.6%
51.7%
2.4%
0.3%
1.0%
23.3%
73.0%
7.7%
6.2%
4.0%
19.9%
62.3%
RPF−seq
RNA−seq
RPF−seq
RNA−seq
Kidney
Liver
unmapped
genome
tRNA
rRNA
cDNA

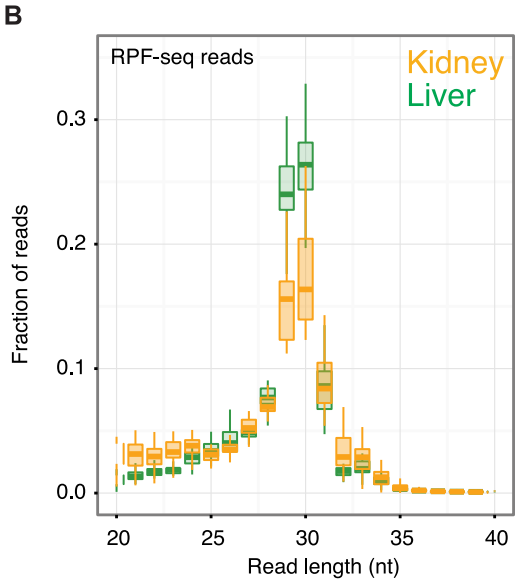
B
RPF-seq reads
Kidney
Liver
Fraction of reads
0.0
0.1
0.2
0.3
20
25
30
35
40
Read length (nt)

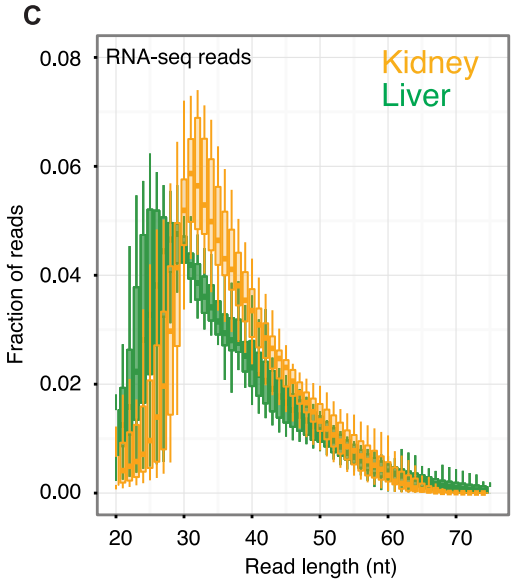
C
RNA-seq reads
Kidney
Liver
Fraction of reads
0.00
0.02
0.04
0.06
0.08
20
30
40
50
60
70
Read length (nt)

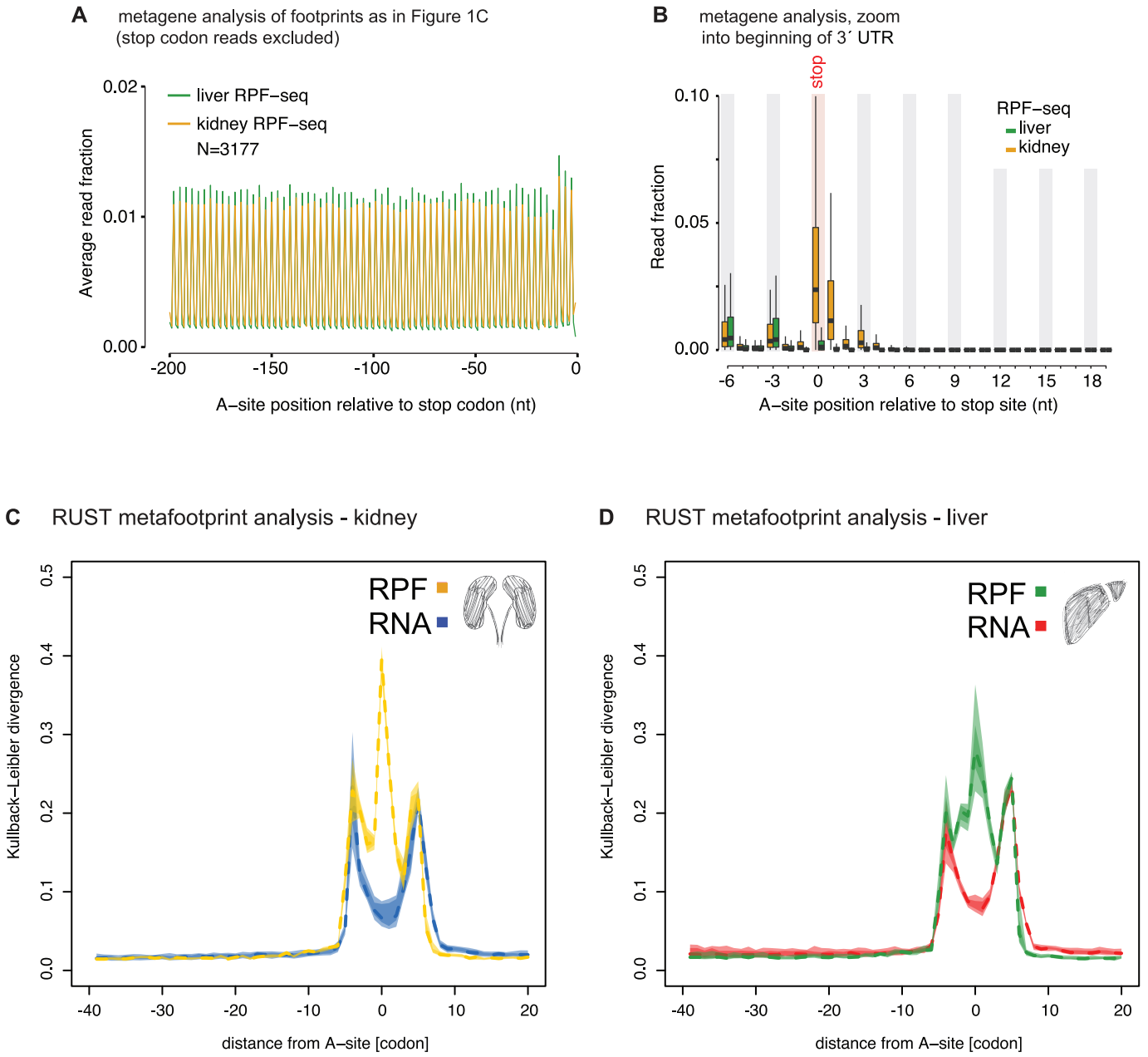
A
metagene analysis of footprints as in Figure 1C
(stop codon reads excluded)
liver RPF–seq
kidney RPF–seq
N=3177
Average read fraction
0.02
0.01
0.00
-200
-150
-100
-50
0
A–site position relative to stop codon (nt)
B
metagene analysis, zoom
into beginning of 3´ UTR
stop
RPF–seq
liver
kidney
Read fraction
0.10
0.05
0.00
-6
-3
0
3
6
9
12
15
18
A–site position relative to stop site (nt)
C
RUST metafootprint analysis - kidney
RPF
RNA
Kullback–Leibler divergence
0.0
0.1
0.2
0.3
0.4
0.5
-40
-30
-20
-10
0
10
20
distance from A–site [codon]
D
RUST metafootprint analysis - liver
RPF
RNA
Kullback–Leibler divergence
0.0
0.1
0.2
0.3
0.4
0.5
-40
-30
-20
-10
0
10
20
distance from A–site [codon]

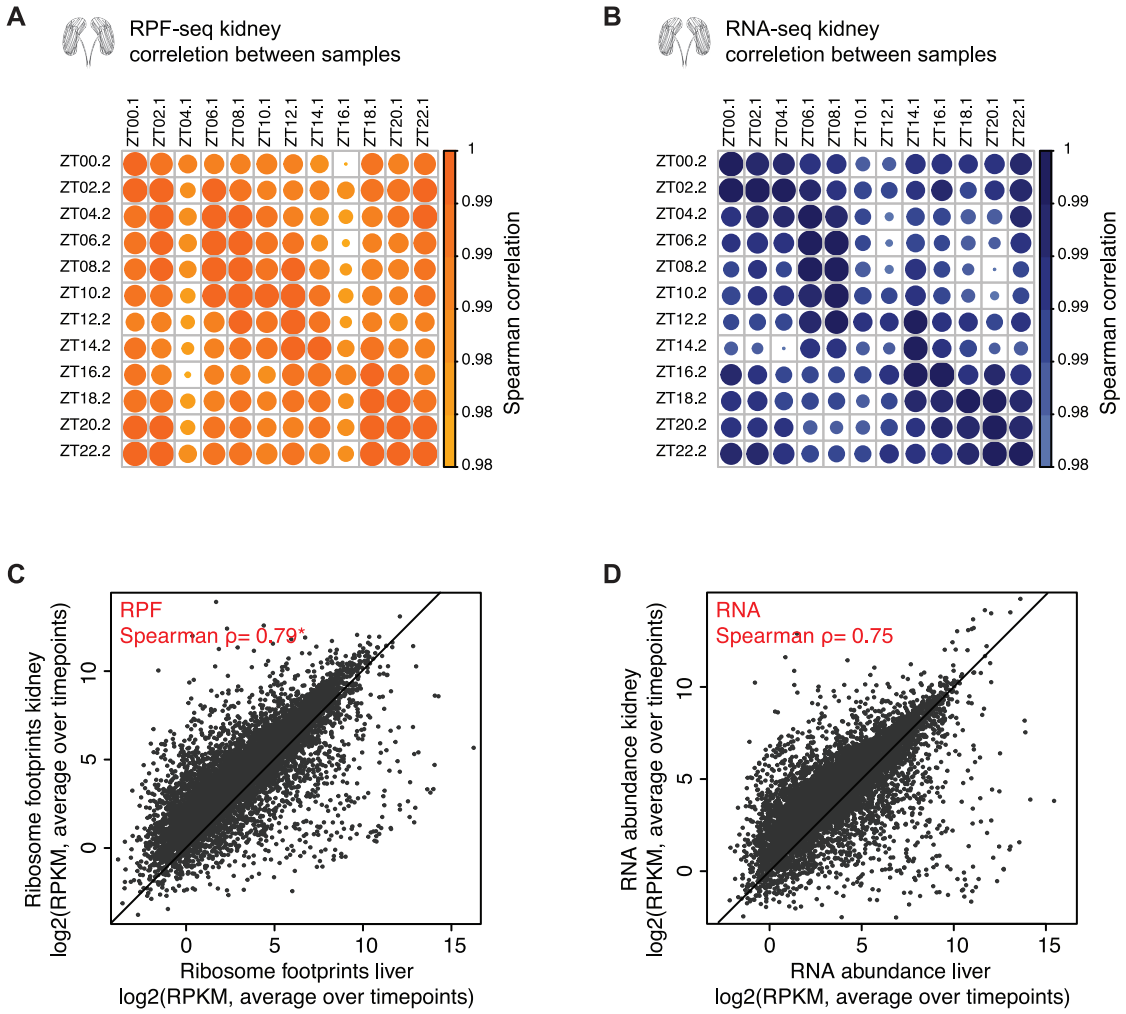

* correlations are significantly different
Steiger test for difference between 2 dependent correlations, Z value=-22.23, p=8.7e-110 (n=10289)

Steiger, J. H. (1980). Tests for comparing elements of a correlation matrix. Psychological Bulletin, 87, 245-251.

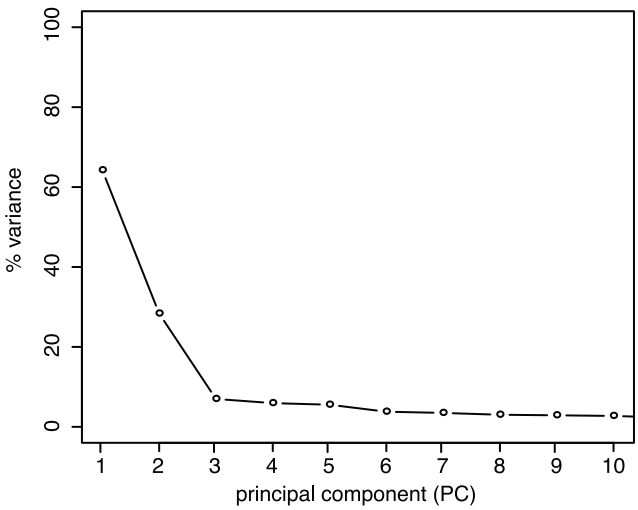
% variance
0
20
40
60
80
100
1
2
3
4
5
6
7
8
9
10
principal component (PC)

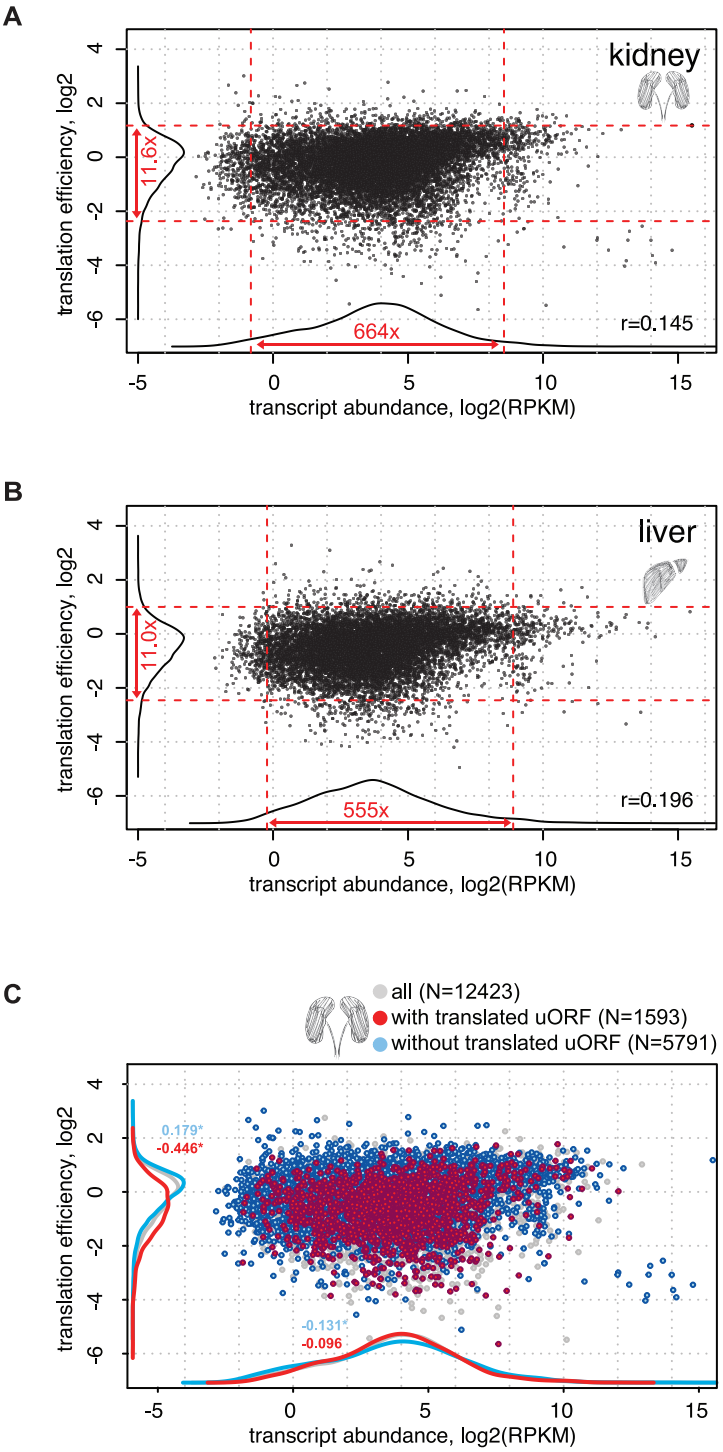
A
kidney
11.6x
664x
r=0.145
translation efficiency, log2
transcript abundance, log2(RPKM)
B
liver
11.0x
555x
r=0.196
translation efficiency, log2
transcript abundance, log2(RPKM)
C
all (N=12423)
with translated uORF (N=1593)
without translated uORF (N=5791)
0.179*
-0.446*
-0.131*
-0.096
translation efficiency, log2
transcript abundance, log2(RPKM)

Measurement errors (MEs), genes binned by expression level

based on all genes (full set, N=10289):

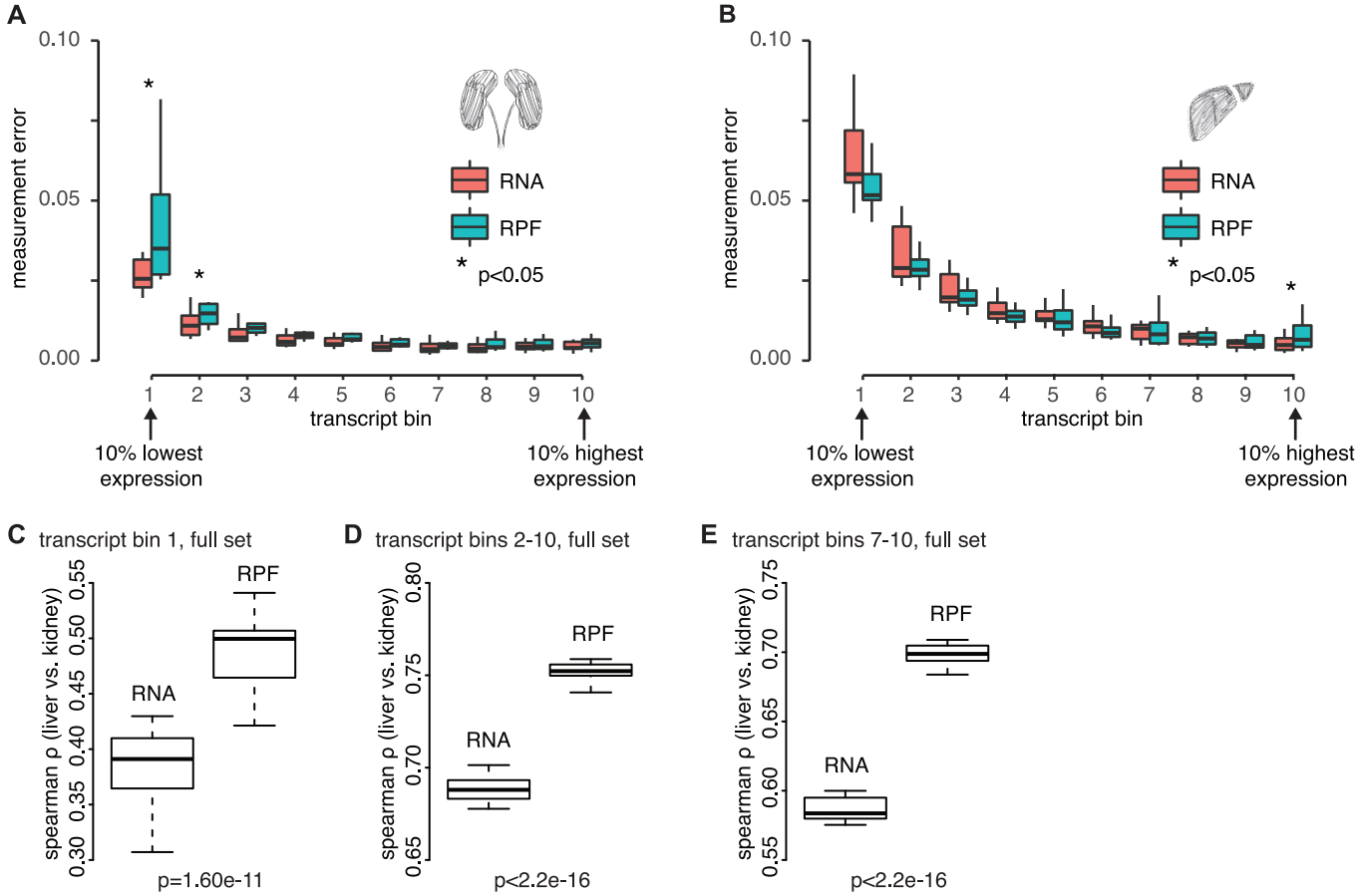

after removal of genes that were most variable in their expression (filtered set, N=9236):

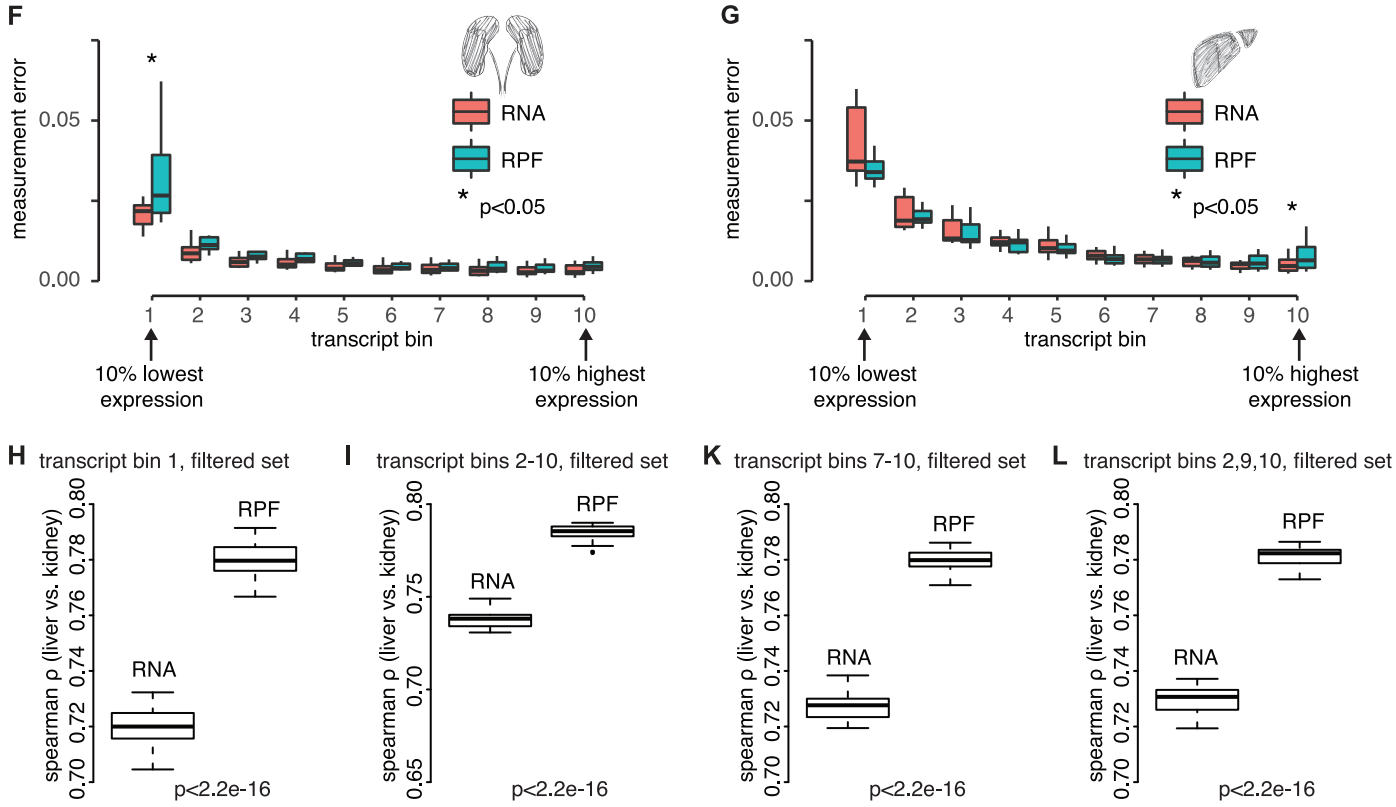

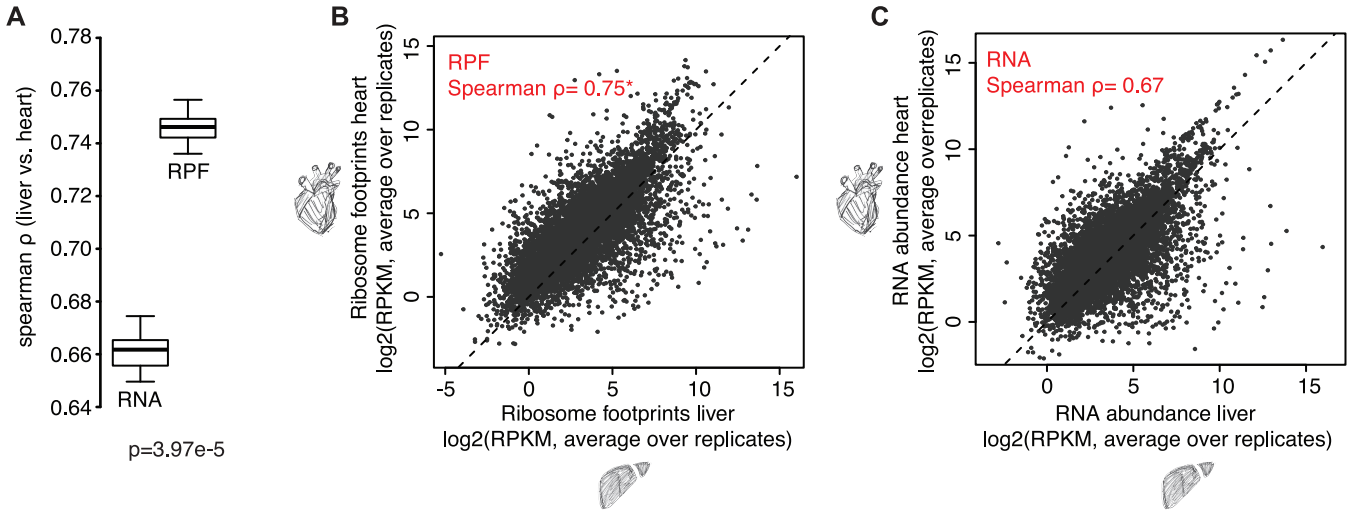

* correlations are significantly different
Steiger test for difference between 2 dependent correlations, Z value=-30.25, p=2.3e-201 (n=9325)

Steiger, J. H. (1980). Tests for comparing elements of a correlation matrix. Psychological Bulletin, 87, 245-251.

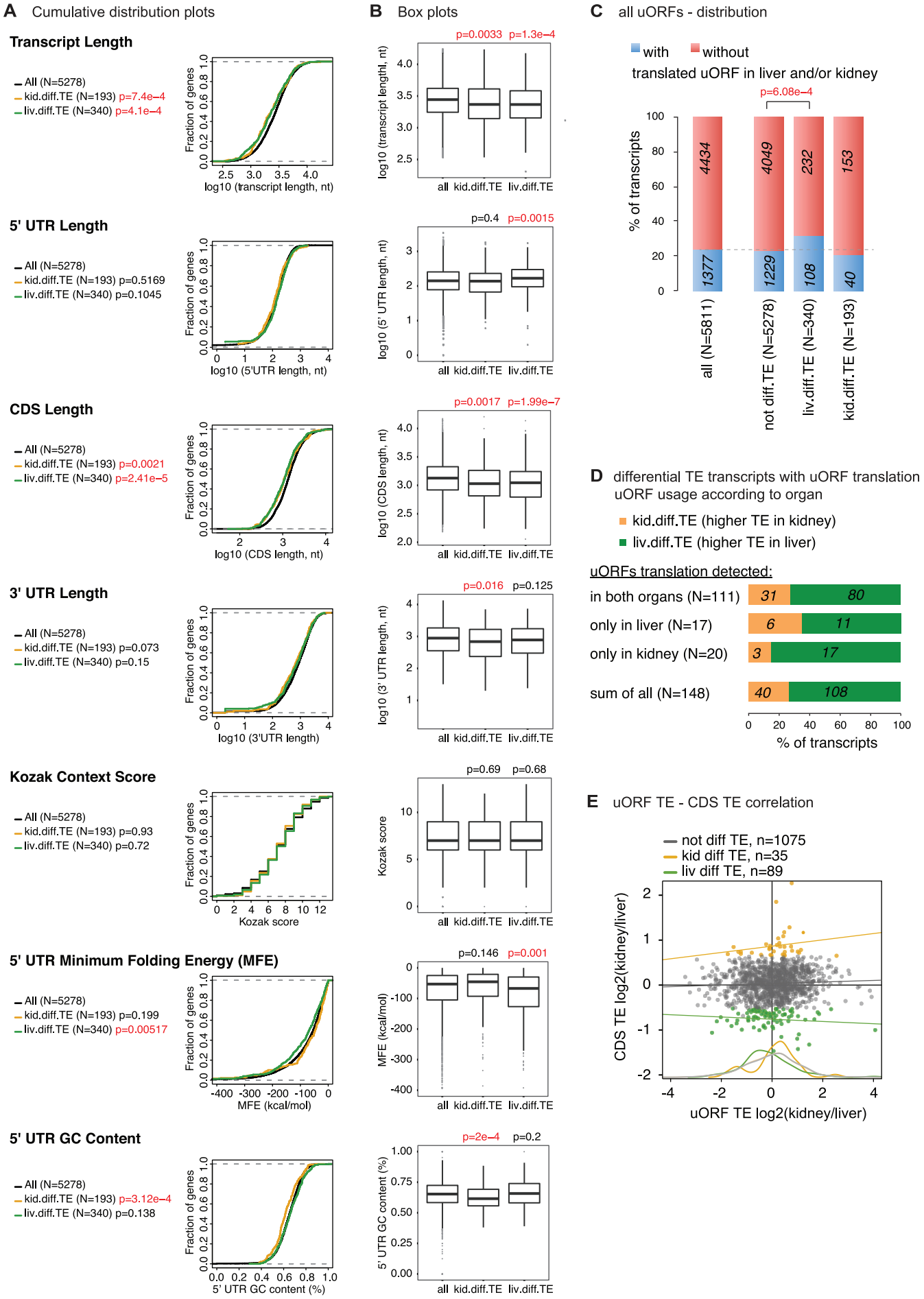
A Cumulative distribution plots
Transcript Length
All (N=5278)
kid.diff.TE (N=193) p=7.4e−4
liv.diff.TE (N=340) p=4.1e−4
Fraction of genes
log10 (transcript length, nt)
5' UTR Length
All (N=5278)
kid.diff.TE (N=193) p=0.5169
liv.diff.TE (N=340) p=0.1045
log10 (5'UTR length, nt)
CDS Length
All (N=5278)
kid.diff.TE (N=193) p=0.0021
liv.diff.TE (N=340) p=2.41e−5
log10 (CDS length, nt)
3' UTR Length
All (N=5278)
kid.diff.TE (N=193) p=0.073
liv.diff.TE (N=340) p=0.15
log10 (3'UTR length)
Kozak Context Score
All (N=5278)
kid.diff.TE (N=193) p=0.93
liv.diff.TE (N=340) p=0.72
Kozak score
5' UTR Minimum Folding Energy (MFE)
All (N=5278)
kid.diff.TE (N=193) p=0.199
liv.diff.TE (N=340) p=0.00517
MFE (kcal/mol)
5' UTR GC Content
All (N=5278)
kid.diff.TE (N=193) p=3.12e−4
liv.diff.TE (N=340) p=0.138
5' UTR GC content (%)
B Box plots
p=0.0033 p=1.3e−4
log10 (transcript lengthl, nt)
all kid.diff.TE liv.diff.TE
p=0.4 p=0.0015
log10 (5' UTR length, nt)
p=0.0017 p=1.99e−7
log10 (CDS length, nt)
p=0.016 p=0.125
log10 (3' UTR length, nt)
p=0.69 p=0.68
Kozak score
p=0.146 p=0.001
MFE (kcal/mol)
p=2e−4 p=0.2
5' UTR GC content (%)
C all uORFs - distribution
with
without
translated uORF in liver and/or kidney
p=6.08e−4
% of transcripts
4434
1377
4049
1229
232
108
153
40
all (N=5811)
not diff.TE (N=5278)
liv.diff.TE (N=340)
kid.diff.TE (N=193)
D differential TE transcripts with uORF translation
uORF usage according to organ
kid.diff.TE (higher TE in kidney)
liv.diff.TE (higher TE in liver)
uORFs translation detected:
in both organs (N=111) 31 80
only in liver (N=17) 6 11
only in kidney (N=20) 3 17
sum of all (N=148) 40 108
% of transcripts
E uORF TE - CDS TE correlation
not diff TE, n=1075
kid diff TE, n=35
liv diff TE, n=89
CDS TE log2(kidney/liver)
uORF TE log2(kidney/liver)

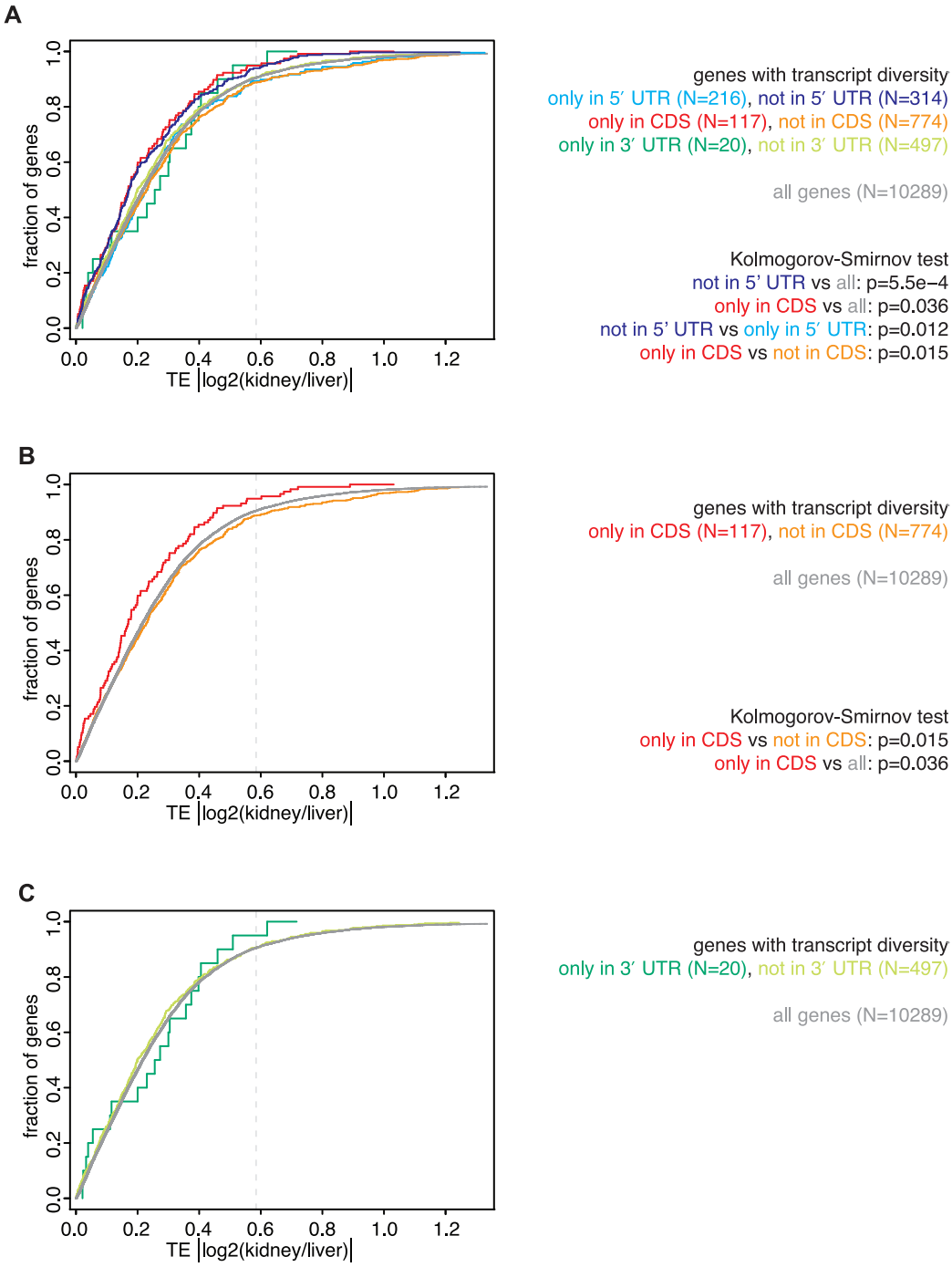
A
fraction of genes
0.0
0.2
0.4
0.6
0.8
1.0
0.0
0.2
0.4
0.6
0.8
1.0
1.2
TE |log2(kidney/liver)|
genes with transcript diversity
only in 5′ UTR (N=216), not in 5′ UTR (N=314)
only in CDS (N=117), not in CDS (N=774)
only in 3′ UTR (N=20), not in 3′ UTR (N=497)
all genes (N=10289)
Kolmogorov-Smirnov test
not in 5' UTR vs all: p=5.5e−4
only in CDS vs all: p=0.036
not in 5' UTR vs only in 5′ UTR: p=0.012
only in CDS vs not in CDS: p=0.015
B
fraction of genes
0.0
0.2
0.4
0.6
0.8
1.0
0.0
0.2
0.4
0.6
0.8
1.0
1.2
TE |log2(kidney/liver)|
genes with transcript diversity
only in CDS (N=117), not in CDS (N=774)
all genes (N=10289)
Kolmogorov-Smirnov test
only in CDS vs not in CDS: p=0.015
only in CDS vs all: p=0.036
C
fraction of genes
0.0
0.2
0.4
0.6
0.8
1.0
0.0
0.2
0.4
0.6
0.8
1.0
1.2
TE |log2(kidney/liver)|
genes with transcript diversity
only in 3′ UTR (N=20), not in 3′ UTR (N=497)
all genes (N=10289)

A Peak phase difference RPF-RNA of rhythmic genes in kidney (N=542)

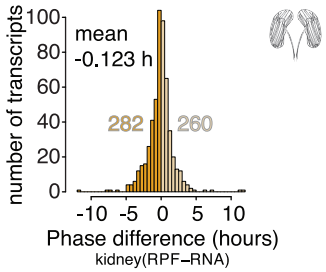

B Peak phase difference RPF-RNA of common rhythmic genes (N=178)

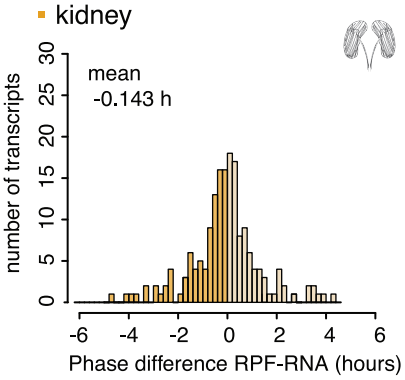

C Peak phase difference RPF-RNA of common rhythmic genes (N=178)

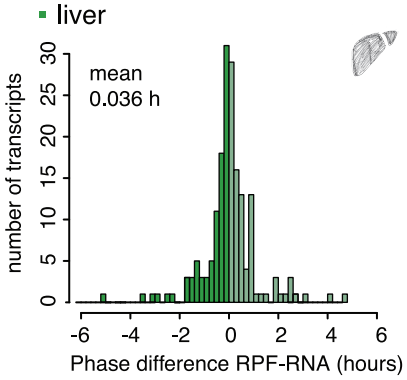

D Peak phase difference (RPF-RNA) in kidney relative to that in liver for the common rhythmic gene set (N=178)

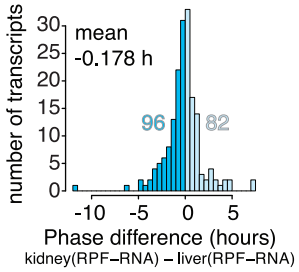

Castelo-Szekely_Supplementary FigS11

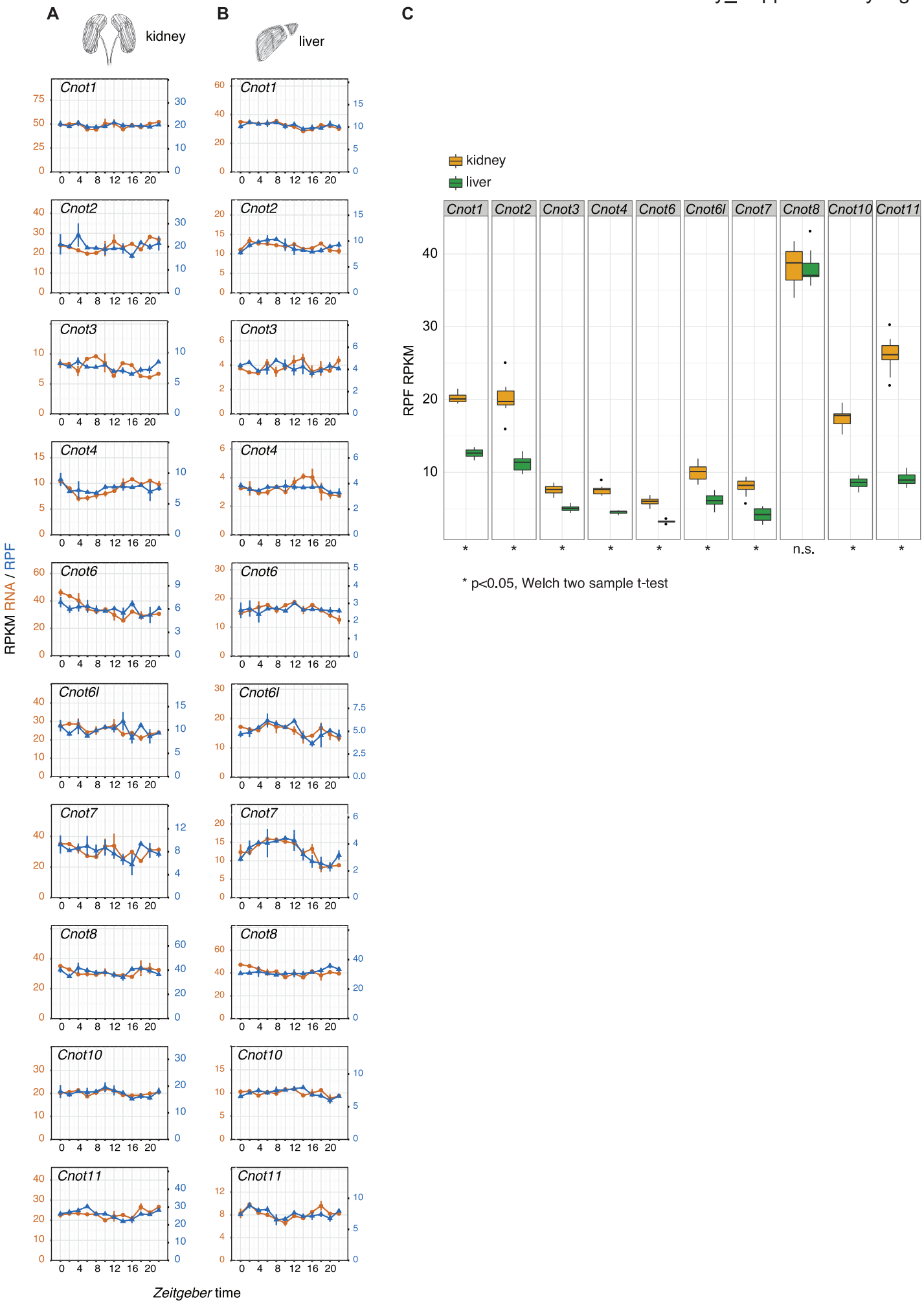

A rhythmic in kidney

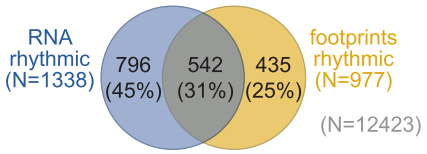

B "RNA only" rhythmic (796 genes)

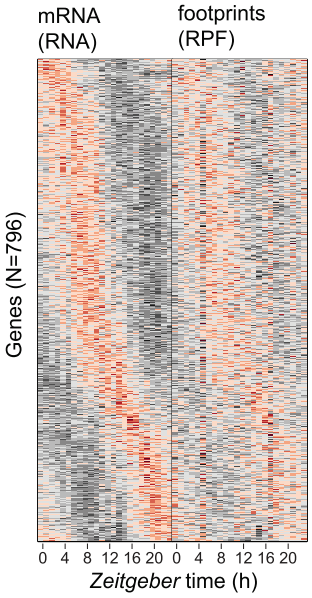

C RNA and RPF rhythmic (542 genes)

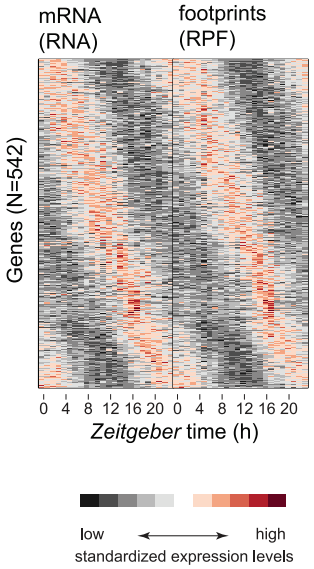

D "footprints only" rhythmic (435 genes)

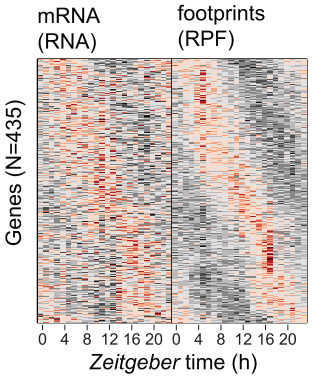

Castelo-Szekely_Supplementary FigS13

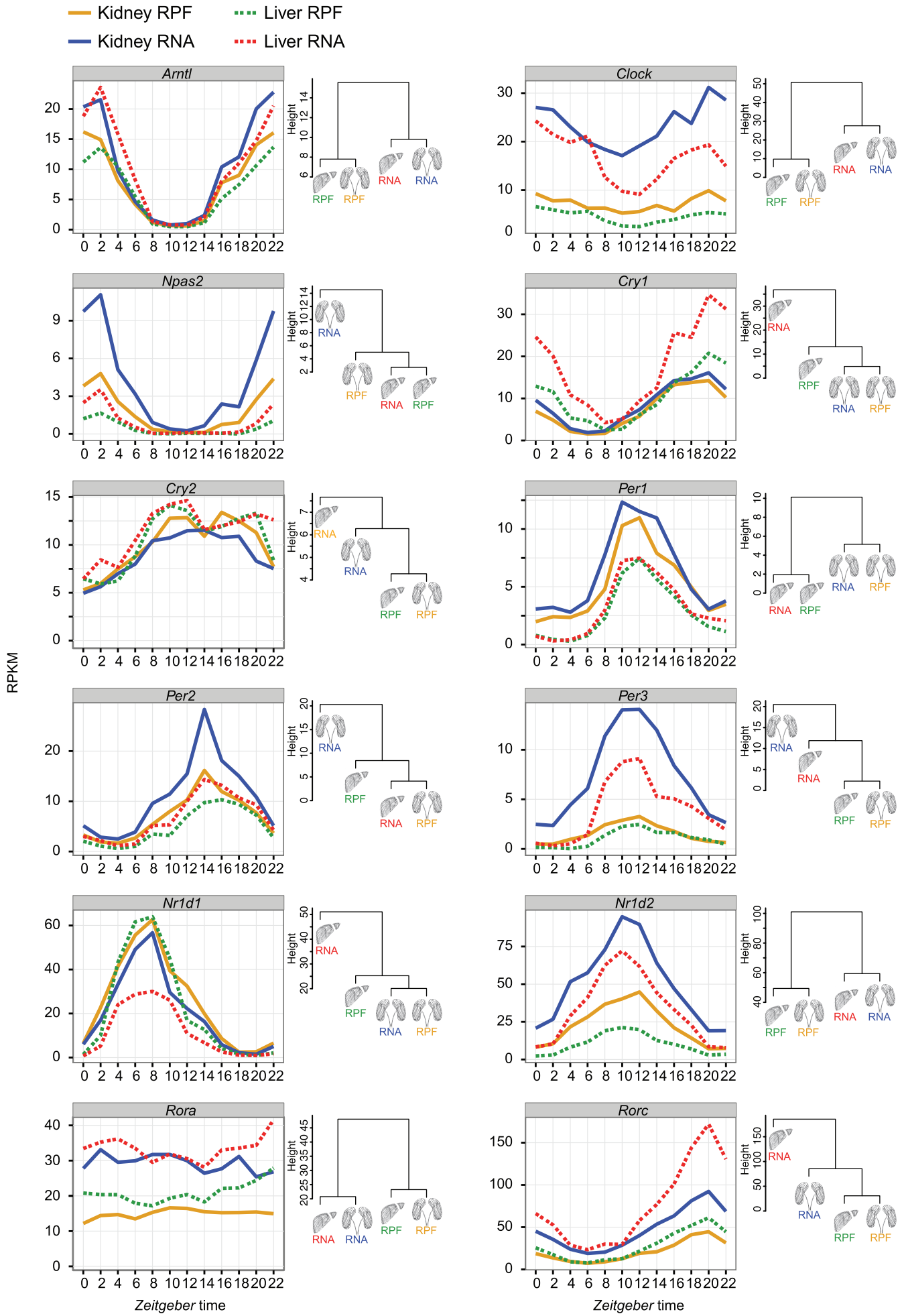

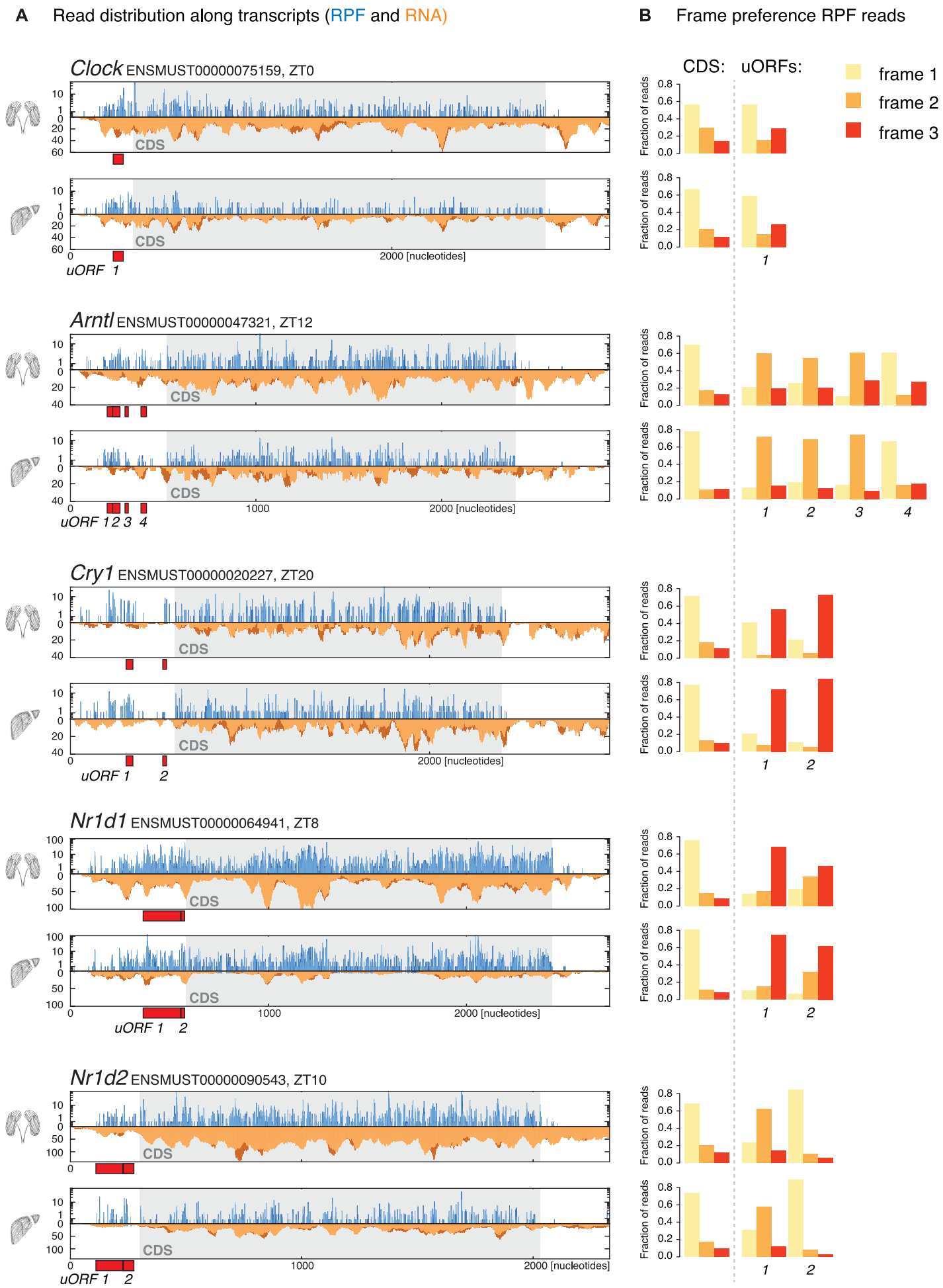
A
Read distribution along transcripts (RPF and RNA)
B
Frame preference RPF reads
CDS:
uORFs:
frame 1
frame 2
frame 3
Clock ENSMUST00000075159, ZT0
CDS
uORF 1
2000 [nucleotides]
Arntl ENSMUST00000047321, ZT12
uORF 1 2 3 4
1000
Cry1 ENSMUST00000020227, ZT20
uORF 1 2
Nr1d1 ENSMUST00000064941, ZT8
Nr1d2 ENSMUST00000090543, ZT10
Fraction of reads